Lithos 205 (2014) 341–358

Contents lists available at ScienceDirect

Lithos

journal homepage: www.elsevier.com/locate/lithos

Age and origin of post collision Baltoro granites, south Karakoram, North Pakistan: Insights from in-situ U–Pb, Hf and oxygen isotopic record of zircons

Munazzam Ali Mahar [a,*], Gweltaz Mahéo [b], Philip C. Goodell [a], Terry L. Pavlis [a]

[a] Department of Geological Sciences, University of Texas at El Paso, El Paso, USA
[b] Université de Lyon, F-69622 Lyon, France Université Lyon 1, Villeurbanne ENS, Lyon CNRS, UMR 5276, Laboratoire de Geologie de Lyon, BAT Géode, 2 rue Dubois, 69622 Villeurvanne, France

ARTICLE INFO

Article history:
Received 28 December 2013
Accepted 5 July 2014
Available online 23 July 2014

Keywords:
India–Asia convergence zone
Post collision magmatism
Miocene granite
Karakoram calc-alkaline crust
Metasomatized Asian mantle
Zircon U–Pb–Hf–O isotopic composition

ABSTRACT

Origin of post collision plutonism is critical to understand the tectonothermal evolution of the over thickened continental crust in collision zones. This has proven difficult to reconcile with the conventional whole rock geochemical and field based studies alone. We report in-situ study of zircon U–Pb, Hf and O isotopes from five samples of the Baltoro Plutonic Unit (BPU) in south Karakoram. The plutonic unit is the western part of the southern Asian margin of the India–Asia convergent zone. Baltoro granites and a biotite-rich enclave yielded similar and overlapping U–Pb ages ranging from 26 to 15 Ma. Hafnium isotopic composition (εHf (0)) is very heterogeneous ranging from −17.1 to +4.4 while the oxygen isotopic composition of the granites is homogeneous with mean $\delta^{18}O$ ranging from 7.2 to 9.4‰. Based on U–Pb geochronology and Hf–O isotopic composition, the involvement of two main sources is suggested (1) Cretaceous calc-alkaline Karakoram crust and (2) Karakoram gneisses. Moreover, possible involvement of metasomatized Asian lithospheric mantle is supported by elevated oxygen composition of granites and identical Hf composition of biotite-rich enclave to the mantle derived Baltoro lamprophyre. However, direct contribution from juvenile pristine mantle is unlikely as no juvenile mantle type Hf and oxygen values were obtained. This also precludes the involvement of southward juvenile arc related component of Kohistan–Ladakh batholith. Our new U–Pb and Hf data are comparable to the Mesozoic Karakoram batholith, Miocene two-mica leucogranites in the Pangong Range and magmatism from the Lhasa terrane in south Tibet, suggesting a genetic link between the Karakoram and the rocks to the east. This magmatic event is best explained by lower crust partial melting promoted by both thermal equilibration following crustal thickening and heat advection by ultrapotassic magmas associated with the breakoff of the Indian continental margin.

1. Introduction

Most of our present understanding about the generation of peraluminous leucogranites in the collision belts of Himalaya–Tibet–Karakoram comes from whole rock geochemical, isotopic, experimental and field based studies (e.g., Deniel et al., 1987; Ferrara et al., 1991; France-Lanord and Le Fort, 1988; Harris and Inger, 1992; Harris et al., 1993; Harrison et al., 1999; Inger and Harris, 1993; Le Fort et al., 1987a,b; Mahéo et al., 2002, 2009; Searle et al., 2010 and references therein). Generation of peraluminous leucogranites is generally attributed to the partial melting of supracrustal pelitic sources (Clemens and Wall, 1981; Stuckless, 1989; Todd and Shaw, 1985) through dominant partial melting reactions, 1) vapor saturated muscovite dehydration melting around 620–650 °C (Thompson, 1982), 2) fluid absent muscovite break down melting at 700–750 °C (Harris et al., 1995) and 3) fluid absent melting of biotite at >750 °C (Le Breton and Thompson, 1988). Based on melting experiments on the metapelites from the High Himalaya Crystalline (HHC) series, fluid-absent melting at around 750 °C and 6–8 kbar by breakdown of muscovite has been suggested to produce the Himalayan leucogranites (Patiño Douce and Harris, 1998). Melting of kyanite-bearing metapelites is also suggested (Goswami et al., 2009). Moreover, high LREE and LILE concentrations and Rb/Sr ratios (1.02–15.85) as well as strong depletion of HREE and HFSE, measured from the Himalayan leucogranites suggested that the Himalayan leucogranites were produced by partial melting of metasedimentary rocks through mica dehydration melting reactions. The structural relation and bulk rock isotopic systematics for Rb, Sr, Nd and O (e.g., Deniel et al., 1987; Ferrara et al., 1991; France-Lanord and Le Fort, 1988) are consistent with a supracrustal origin. However, involvement of igneous (i.e., granitic) protolith in the source region has also been suggested (e.g., Ferrara et al., 1991; Pognante, 1992). Although detailed studies have been performed on the partial melting of the underthrusting Indian plate, very few studies were done on the partial melting of the Asian plate following crustal thickening.

In this study we focus on the origin of the Baltoro Plutonic Unit (BPU). This plutonic body outcrops in south Karakorum (Pakistan),

* Corresponding author.

http://dx.doi.org/10.1016/j.lithos.2014.07.014
0024-4937/

the western prolongation of southern Tibet, and part of the southern margin of the Asian plate (Fig. 1). The BPU is forming the southeastern part of the larger Karakoram Axial Batholith (Fig. 1) and has been variously interpreted in the last two decades. Debon et al. (1986) suggest that the Baltoro granite formation was related with both crustal and mantle melting during Indian continental subduction. Later, based on Pb, Sr and Nd isotopic composition as well as zircon and monazite inheritance, Schärer et al. (1990) proposed a strong crustal input; that is, more than 70% of the magmas derived from the meta-sedimentary rocks of the Karakoram Metamorphic Complex (KMC). Lower initial $^{87}Sr/^{86}Sr$ ratio of Baltoro granites (0.71–0.72) compared to Himalayan leucogranites (0.74–0.82) is attributed to the partial melting of metapelites through vapor absent biotite dehydration melting around 850 °C at lower crustal depths (Bhalla et al., 1994; Crawford and Windley, 1990; Rex et al., 1988; Searle et al., 1992, 2010). On the other hand, partial melting of deep seated dioritic to granodiorite and metabasalts (Cretaceous, calc-alkaline rocks) has been suggested (Mahéo et al., 2002, 2009). Thus, multiple sources have been proposed for the same rocks with similar whole rock isotopic signature. Similarly, multiple sources have been proposed for the Karakoram Shear Zone leucogranites (geochemically comparable to the Baltoro granites) exposed along the Karakoram Fault, southeast of the Baltoro region (Fig. 1; Pangong Range). These sources include the proximal Karakoram and Ladakh batholiths (Reichardt et al., 2010; Weinberg et al., 2009), subducted Indian crust (Leech, 2008), or a combination of the two (Horton and Leech, 2013; Ravikant et al., 2009).

From these past studies, it is evident that the precise characterization of magma source components and petrogenetic processes for the production of post collision granites is difficult to constrain by whole rock geochemical and isotopic data. Such data provide averaged information and are sensitive to post-crystallization, mineralogical and chemical modification (e.g., Appleby et al., 2010; Hawkesworth and Kemp, 2006; Kemp and Hawkesworth, 2003; Kemp et al., 2007).

The capability to explore the micro-scale in-situ U–Pb and Lu–Hf isotopic records of zircons has revolutionized granite petrology, particularly with reference to the source region history and magma mixing (e.g., Andersen and Griffin, 2004; Belousova et al., 2006; Boekhout et al., 2013; Flowerdew et al., 2006; Goodge and Vervoort, 2006; Griffin et al., 2002; Kemp et al., 2005, 2009a; Phillips et al., 2011; Shaw and Flood, 2009; Zeh et al., 2007). However, the Hf isotopic system alone sometimes is unable to constrain the involvement of mantle magmas in granite petrogenesis (e.g., Hawkesworth and Kemp, 2006; Kemp et al., 2007, 2008). The oxygen isotopic record from zircon grains provides more robust constraints to investigate the involvement of mantle-derived magmas (Valley et al., 2005) in granite formation (Appleby, 2008; Appleby et al., 2010; Gagnevin et al., 2011; Hawkesworth and Kemp, 2006; Kemp et al., 2006, 2007, 2009b; Miles et al., 2014 and references therein). That is, U–Pb data can be used to determine the emplacement age of granites and the relative components of mantle and crustal sources can be constrained by O and Hf isotope data.

To understand the petrogenesis of the post collision Baltoro granites, we document the in-situ integrated isotopic record (U–Pb, Hf and oxygen) of zircons. First, we describe the isotopic composition of the Baltoro granites and then these values are correlated with the spatially and temporally related lithotectonic units. Finally, based on U–Pb ages

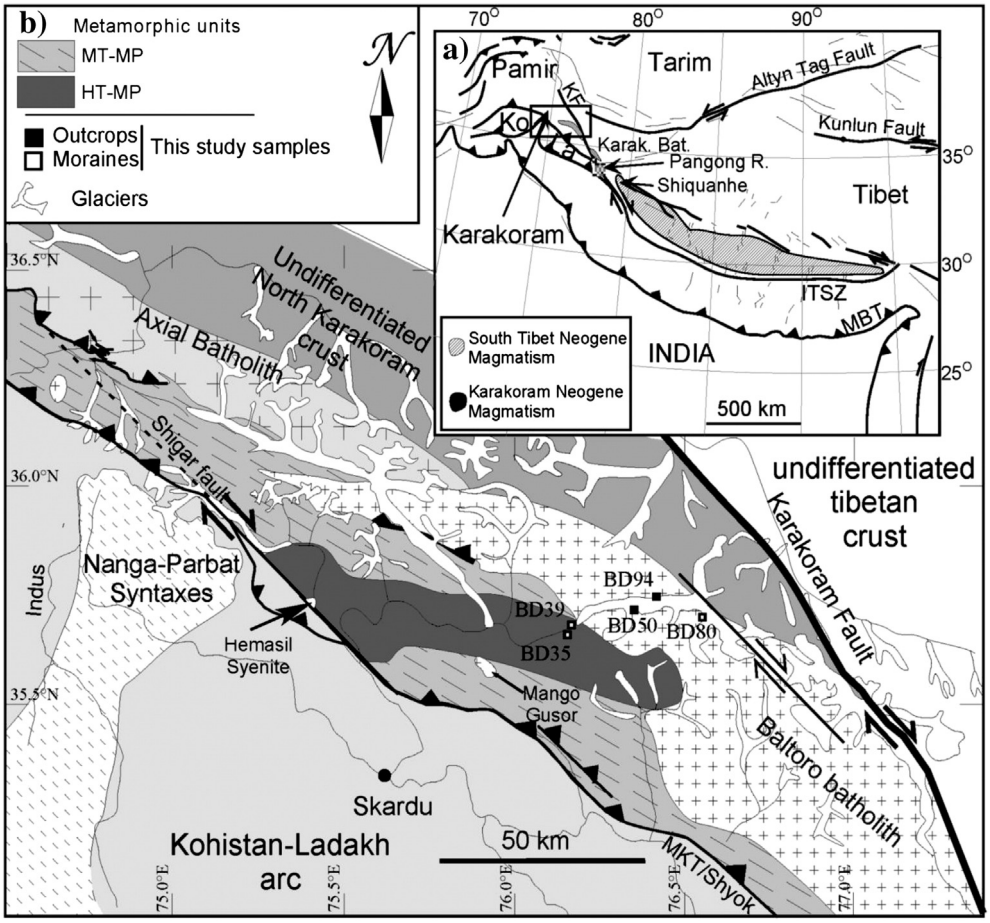

Fig. 1. South Karakoram geological map and sample location. MBT: Main Boundary Thrust, MKT: Main Karakoram Thrust, ITSZ: Indus Tsangpo Suture Zone, KF: Karakoram Fault, Ko: Kohistan, La: Ladakh GC: Garam Chashma.
After Mahéo et al. (2004) and Pêcher et al. (2008).

and isotope composition, we propose a post collision Miocene tectonic configuration at the southern margin of the Asian plate. The zircon U–Pb data suggest that the Baltoro Plutonic Unit is Miocene in age (26–15 Ma) while Hf and O isotopic composition indicates the involvement of multiple sources, and partial melting of infra and supracrustal sources is induced by biotite and amphibole dehydration melting with some input from metasomatised mantle. Additional heat to melt the lower crust is provided by ultrapotassic magma intrusions. The latter are related to the breaking off of Indian continental lithosphere beneath Karakoram.

2. Geology, field relations and previous interpretations

The Karakoram terrane is defined as Precambrian to Cambro-Ordovician basement with a Paleozoic history suggesting its Gondwana affinity (Gaetani, 1997). The Karakoram terrane is mostly located to the west of, and separated from southern Tibet by the dextral Karakoram Fault (Fig. 1). However, part of this terrane, namely the Karakoram batholith, has been recognized east of the Karakoram fault (Srimal et al., 1987; Fig. 1).

North Karakoram is mostly composed of Permian to Early Cretaceous sedimentary rocks, representing deposition at a passive margin environment associated with the opening of the Tethys Ocean (Gaetani and Garzanti, 1991). South Karakoram marks the active continental margin of southern Asia (e.g., Coward et al., 1986; Debon et al., 1987; Le Fort et al., 1983; Searle et al., 1987). Three major, successive thermotectonic events have been recognized. First, calc-alkaline plutonic rocks intruded during the Cretaceous, formed the Axial Batholith (Crawford and Searle, 1992; Debon and Khan, 1996; Debon et al., 1987) (Fig. 1). Similar rocks have also been observed in the eastern part of the Karakoram batholith that is east of the Karakoram Fault (Ravikant et al., 2009; Srimal et al., 1987). This subduction is also responsible for the Mid-Cretaceous opening of the Shyok back-arc basin separating the Karakoram margin from the southern Kohistan arc (Rolland et al., 2000, 2002). Second, northward subduction of the Shyok back-arc induced by the collision of the south Karakoram with the Kohistan–Ladakh oceanic arc along the Shyok Suture Zone during late Cretaceous formed the southern margin of Eurasia (Petterson and Windley, 1992; Rolland et al., 2000; Weinberg et al., 2000). This collision, followed by the collision between the Kohistan–Ladakh arc and the Indian plate (at ~50 Ma; e.g., De Sigoyer et al., 2000; Dewey et al., 1989; Green et al., 2008; Patriat and Achache, 1984; Zhu et al., 2005) led to crustal shortening by stacking. The crustal thickening resulted in the development of medium-temperature, medium-pressure metamorphism (Fraser et al., 2001; Lemennicier et al., 1996; Rolland et al., 2001; Searle et al., 1989). The final tectonothermal event was post thickening resulting in high-temperature–low-pressure metamorphism and partial melting (Bertrand et al., 1988; Lemennicier et al., 1996; Mahéo et al., 2004; Rolland et al., 2001; Searle et al., 1989, 2010). The latter has been associated with the emplacement of late orogenic potassic magmas (Mahéo et al., 2002, 2009). The main post-thickening magmatic unit is the Baltoro Plutonic Unit (BPU, Fig. 1), which crops out for >300 km along strike from the Snow Lake–Biafo glacier region to the Nubra–Pangong Ranges in Ladakh (Fig. 1; Mahéo et al., 2009; Searle et al., 1989, 2010 and references therein). Based on U–Pb zircon ages, this batholith has been emplaced between 26 and 13 Ma (e.g., Parrish and Tirrul, 1989; Schärer et al., 1990; Searle et al., 2010).

2.1. Baltoro Plutonic Unit

The geology, geochemistry and field relations of the Baltoro plutonic unit are discussed in detail elsewhere (Bertrand and Debon, 1986; Mahéo et al., 2009; Searle et al., 1992, 2010 and references therein). Here we summarize the major feature of the magmatic rocks of the unit.

The Baltoro granites are Miocene in age (26–13 Ma) and mainly consist of two end member granitoids: 1) biotite-rich, less-differentiated, water undersaturated, large ion lithophile element (LILE)-enriched non-minimum melt biotite monzogranites and 2) leucogranites, which are the fractionated product of monzogranites. The granites consist of quartz–K-feldspar–plagioclase–biotite ± muscovite ± garnet, with accessory titanite, zircon, monazite and opaques.

Granites in the BPU are mildly peraluminous and calc-alkaline to alkali-calcic. Leucogranites dominantly fall in ferron field while biotite monzogranites show transition from magnesian to ferron with increasing SiO_2 content (Fig. 2). Major element geochemistry of Baltoro granites is comparable to the Neogene leucogranites in the Pangong Range (Karakoram Shear Zone) and eastern part of Karakoram batholith (i.e., Nubra Valley and Shyok suture zones; Reichardt et al., 2010) and less evolved than the strongly peraluminous High Himalayan Granites (HHG) (Fig. 2, for location see Fig. 1).

The concentrations of MgO, CaO and FeO_T decrease from biotite monzogranite to leucogranites, these coupled with high concentration of SiO_2 indicate differentiation from more primitive type magmas suggesting derivation from mafic protolith: 1) either by extensive differentiation of mantle derived magmas or 2) by partial melting of basalt-dioritic type sources (e.g., Mahéo et al., 2009). Higher concentration of Ba and Sr, low Rb/Sr and K/Sr ratios (0.1–3.9 and 80.3, respectively) coupled with SiO_2 enrichment has been attributed to the partial melting of plagioclase bearing sources in the presence of residual amphibole (Mahéo et al., 2009; Petford and Atherton, 1996). Based on the REE pattern (low HREE and higher LREE) and Y concentration, the presence of garnet in the source region or sequestering of garnet from the melt by fractional crystallization has been suggested (Mahéo et al., 2009).

Neogene partial melting of previously metasomatised mantle is evident by whole rock isotopic and geochemical signatures of lamprophyres (22, 24 Ma) in south Karakoram and the Baltoro region (Mahéo et al., 2002, 2009). The generation of lamprophyres (32 Ma and 22–24 Ma) both older and younger than the Baltoro granites (Rex et al., 1988; Searle et al., 2010) has been explained by slab break-off of the Indian continental lithosphere facilitating asthenospheric mantle upwelling resulting in melting of the previously metasomatised Asian lithospheric mantle (Mahéo et al., 2002, 2009; Rolland et al., 2001). Hemasil syenite (9 Ma), which is one of rock assemblages in the domal structure in the south Karakoram (Fig. 1), has been interpreted as generated by partial melting of depleted mantle in a late-stage metasomatic event that resulted from upwelling and adiabatic decompression of depleted mantle (Mahéo et al., 2009). Also, the low abundance of tourmaline, high crystallization temperature and the batholithic size of the assemblage suggests that in contrast to the High Himalayan granites (HHG), Baltoro granites are produced by melting of lower crustal sources and involvement of mantle magmas is likely in providing the additional heat (Mahéo et al., 2009).

3. Sample descriptions

In the present work, we study the samples collected by F. Debon in 1984 from the Baltoro plutonic unit. The Karakoram igneous-metamorphic terrane is highly glaciated with a cluster of several of the tallest peaks (>7000 m) in the world. Four granite samples and one dark biotite rich granodioritic enclave within the biotite monzogranite was selected to study the zircon isotopic record. The samples were collected traversing west to east along Braldu River–Baltoro glacier from Dumordul–Braldu confluence (35°41′N, 75°58′E) in the west to Biange glaciar in the east (35°45 N, 76°22′E) (Fig. 1). Two samples (BD50 & BD94) have been collected directly from outcrops whereas three samples (BD35, 39 & 80) come from moraine deposits related to the Baltoro Glacier (Fig. 1). In the following, field relationships, petrography and zircon morphology of the samples is briefly described. The cathodoluminescence (CL) images of all the analyzed zircons with labeled isotopic data can be found in data repository (DR — Fig. 1). Selected grains with labeled isotopic data are shown in (Fig. 3).

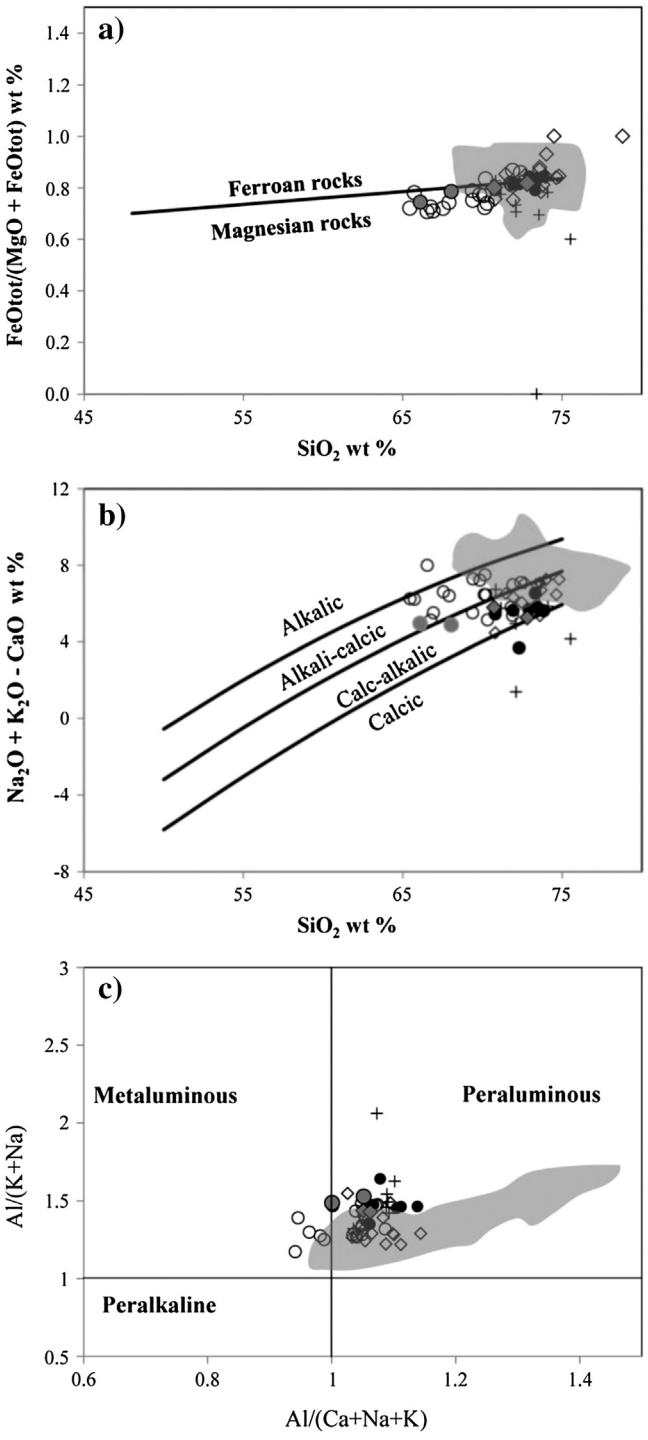

Fig. 2. Geochemical characteristics of the Baltoro granites. (a, b, c) Geochemical classification of granites (Frost et al., 2001; Maniar and Piccoli, 1989); open circles: Baltoro monzogranite, open diamonds: Baltoro leucogranite (Debon et al., 1986; Mahéo et al., 2009; Searle et al., 1992), solid circles: Karakoram batholith leucogranite (Reichardt et al., 2010), plus symbol: Pangong Range leucogranites (Reichardt et al., 2010), gray field: High Himalayan granites (Guo and Wilson, 2012; Searle et al., 1997; Singh, 2013; Visona and Lombardo, 2002). Gray-filled diamonds and circles are the samples studied in the present work.

3.1. Biotite monzogranite (BD39 & BD80)

BD80 and BD39 are the biotite rich monzogranites (referred to as monzonites by Searle et al., 2010 and references therein) collected from the Dumordul–Braldu confluence approximately 6 km northwest of Bardumal village and northern flank of Braldu River, 4 km east of Paiu village at 35°41′N, 76°08.2′E, respectively (Fig. 1). Plagioclase, quartz, biotite, titanite and magnetite are the major minerals. The granites are enriched in accessory phases like zircon, apatite and monazite which are dominantly included within the biotite. Geochemically, sample BD80 is magnesian, alkali-calcic and at the line differentiating the metaluminous from the peraluminous granites while sample BD39 is relatively silica enriched, magnesian, calc-alkaline and peraluminous (Fig. 2a–c). CL images show that the zircons are generally magmatic and inclusion free, showing strong oscillatory zoning from rim to core. In one sample sector zoning is also observed (Fig. 3). Rims are generally darker while the cores are brighter. Inherited cores have diffused primary zoning or no zoning at all. Recrystallization of the partially melted core is evident by dissolution structures like corrosion and embayed surfaces. The length of zircon crystals ranges from 200 to 400 μm. The zircons are larger with aspect ratio of 1:3.

3.2. Garnet-two mica leucogranites (BD50 and BD35)

Two samples BD50 (low MgO) and BD35 (high MgO) are more differentiated garnet-two mica leucogranites and were collected 2 km east of Liliwa village at 35°42.75′N, 76°15′E and on the southern flank of Braldu River, 2.75 km southeast of Paiu village at 35°39.25′N, 76°07.50′E, respectively (Fig. 1). Both samples are higher in SiO_2 (>70%), magnesian (BD35) to ferron (BD50), calc-alkaline and peraluminous (Fig. 2a–c). The leucogranite samples are enriched in accessory phases like zircon, apatite and monazite.

Zircons are inclusion free, showing strong oscillatory zoning from rim to core (Fig. 3). Some zircons show more than two or three growth domains and a clear core to rim distinction can be observed. The relatively bright rounded, homogeneous cores with no zoning are referred here as metamorphic cores. Some cores are corroded, and dissolution–recrystallization structures are conspicuous. The length of zircon crystals ranges from 200 to 300 μm with aspect ratios of 1:3 & 1:2.

3.3. Biotite-rich enclave (BD94)

BD94 is a dark, biotite-rich enclave in the monzogranite, collected from the south of Biange glacier at 35°46′N, 76°24′E. The sample has abundant biotite and green amphibole, plagioclase, quartz and K-feldspar. Based on its mineralogy, this sample is interpreted as a high potassium magmatic rock that could be a plutonic equivalent of lamprophyres. Such high potassium, biotite-amphibole enriched enclaves have also been reported from the Variscan collision belt and similar to the BD94 are found in the monzogranites/monzonites in Mórágy Hills and Tisia terrane (South Hungary). These lamprophyre-derived enclaves are named as the melamonzonite, amphibole biotite melasyenite, rarely amphibole meladiorite or redwitzite (Buda and Dobosi, 2004; Le Maitre et al., 1989 and references therein).

Zircons are fine grained showing perfect magmatic oscillatory zoning with occasional inherited rounded cores. Zircons show variable structures from being more elongated with 1:3 aspect ratio to almost rounded with strong oscillatory zoning, sector zoning and mineral inclusions can also be observed. The length of zircon crystals ranges from 100 to 250 μm with aspect ratios of 1:2 and 1:3 (Fig. 3).

4. Results

The zircon U–Pb and Hf isotopic measurements were performed by LA-MC-ICP-MS at the LaserChron laboratory, University of Arizona. The followed analytical methods for U–Pb and Hf isotopic measurements are fully described in Gehrels et al. (2008) and Cecil et al. (2011), respectively. The oxygen isotope measurements were carried out at WiscSIMS facility, University of Wisconsin using CAMECA IMS-1280 SIMS, following the method described by Kita et al. (2009) and

Valley and Kita (2009). Details of the methods are given in Appendix A in the supplementary material.

The U–Pb and Hf data are listed in supplementary data Tables T1 and T2, respectively. Summarized oxygen data are listed in Table T3 while Table T4 shows the oxygen data along with standards and analytical parameters. The mean $\delta^{18}O$ and weighted mean (WM) epsilon Hf values shown in the tables and figures are at 2σ. Summary of the isotopic data (along with number of samples analyzed), presenting the WM ages, inherited age range, mean oxygen and WM Hf isotopic record for individual sample is made available in Table. 1. Note that uncertainties given in the supplementary U–Pb data (Table T1) are reported at the 1-sigma level, and include only measurement errors. Systematic errors are as follows (at 2-sigma level): 1.2% ($^{206}Pb/^{238}U$) & 0.8% ($^{206}Pb/^{207}Pb$).

4.1. U–Pb geochronological data

4.1.1. Overgrowth ages

All the zircon overgrowths show low U/Th ratios indicative of a magmatic origin and their U–Pb isotopic ratios plot on the concordia line (Fig. 4). Both leucogranite samples, BD50 and BD35 yielded identical WM ages of 21.6 ± 0.5 Ma (n = 7, MSWD = 0.63) and 21.6 ± 0.3 Ma (n = 8, MSWD = 0.78), respectively (Fig. 4a & b). However, low Mg leucogranite shows a slightly younger population with a WM age of 18.2 ± 0.4 Ma (n = 10, MSWD = 0.45) (Fig. 4a). One spot from high Mg leucogranite (BD35-22) also yielded an age of 18.3 ± 0.8 Ma, identical to the younger population of BD50 leucogranite. BD35-24 spot yielded the youngest age of 15 ± 0.6 Ma in this study. One rim analyses (BD35-33) gave a concordant age of 76 ± 3.4 Ma. The zircons from

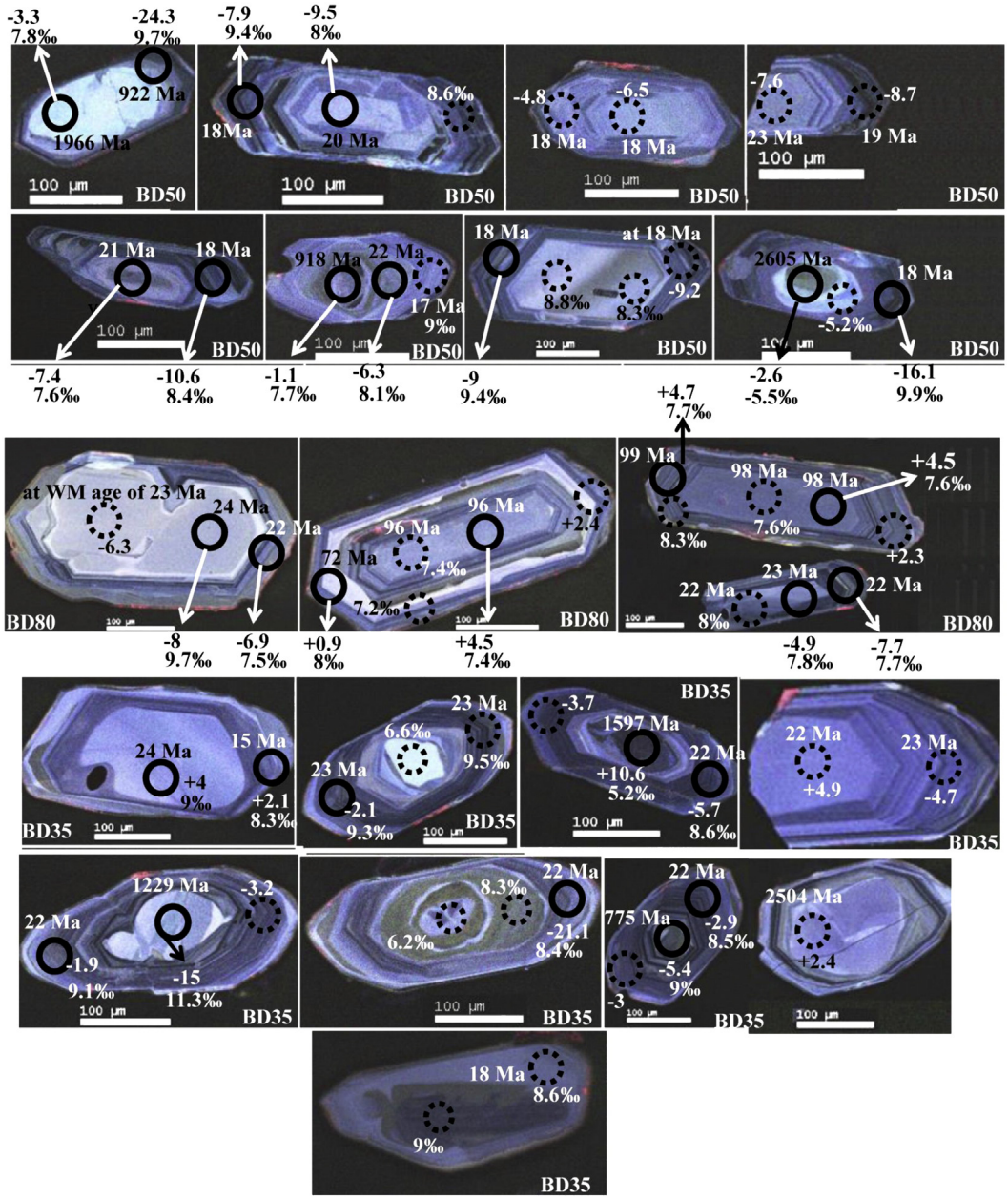

Fig. 3. Representative analyzed zircons and location of the analytical spots. X‰: $\delta^{18}O$; XMa: U–Pb age; X: εHf (t). Note that bold circles are the spots where both Hf and oxygen isotopic analyses were performed along with U–Pb ages.

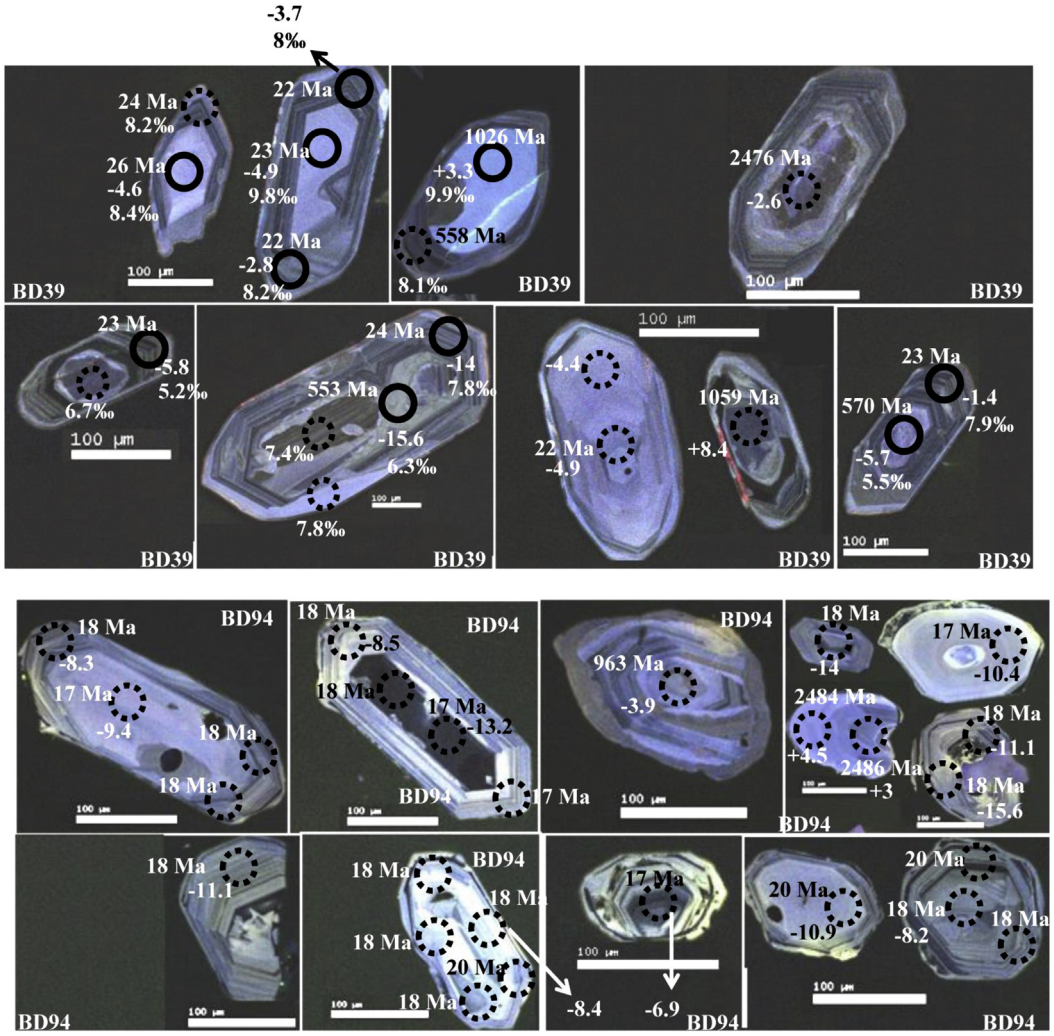

Fig. 3 (*continued*).

two biotite monzogranite samples, BD39 and BD80 yielded identical WM ages of 22.5 ± 0.3 Ma (n = 8, MSWD = 0.64) and 22.5 ± 0.4 Ma (n = 8, MSWD = 0.41), respectively (Fig. 4c & d). Two magmatic zircons from BD80 with strong oscillatory zoning yielded a WM age of 97.2 ± 2.4 Ma (n = 5, MSWD = 0.3). A coherent group of ages from the biotite rich enclave placed a WM age of 17.7 ± 0.14 Ma (n = 27, MSWD = 0.58) (Fig. 4e). This coincides with the younger population from leucogranite sample BD50.

4.1.2. Inherited ages

Inherited ages from the studied zircons are shown as the concordia plots in (Fig. 5). Analyses on six inherited cores from leucogranite BD50 presented highly variable $^{206}Pb/^{207}Pb$ ages: three cores yielded discordant ages ranging from 918 to 975 Ma. Two spots (BD50-31b and BD50-26) show strong discordance while the other four show almost <10% discordance. Three cores yielded older, discordant $^{206}Pb/^{207}Pb$ ages from 1966 to 2605 Ma (Fig. 5a). The uranium

Table 1
Summary of isotopic data.

Rock type	LA-ICP-MS U–Pb (zircon) WM ages	LA-ICP-MS WM εHf (0) at 95% conf	SIMS $\delta^{18}O$ (‰, VSMOW)
Low Mg leucogranite (BD50) younger magmatic event	18.2 ± 0.4 Ma (n = 10, MSWD = 0.45)	−8.1 ± 1.6 (n = 8, MSWD = 2.4)	9.4 ± 1.0 (2SD)
Low Mg leucogranite (BD50) older magmatic event	21.6 ± 0.5 Ma (n = 7, MSWD = 0.63)	−8.7 ± 1.4 (n = 7, MSWD = 1.3)	8.4 ± 1.4 (2SD)
Inheritance (BD50)	922–2605 Ma (n = 6)	−58.6 to −21.4 (n = 5)	8.1 ± 3.2 (2SD)
High Mg leucogranite (BD35) magmatic zircons	21.6 ± 0.3 Ma (n = 8, MSWD = 0.78)	−4.0 ± 0.9 (n = 11, MSWD = 0.67)	8.9 ± 0.7 (2SD)
Inheritance (BD35)	775–2504 Ma (n = 5)	−53.9 to −22.5 (n = 5)	9.2 ± 2.8 (2SD)
Monzogranite (BD80) younger magmatic event	22.5 ± 0.4 Ma (n = 8, MSWD = 0.41)	−7.6 ± 1.0 (n = 7, MSWD = 0.65)	7.8 ± 0.4 (2SD)
Monzogranite (BD80) older magmatic zircons	97.2 ± 2.4 Ma (n = 5, MSWD = 0.3)	0.9 ± 1.0 (n = 6, MSWD = 1.13)	7.7 ± 0.8 (2SD)
Monzogranite (BD39) magmatic zircons	22.5 ± 0.3 Ma (n = 8, MSWD = 0.64)	−4.5 ± 0.9 (n = 9, MSWD = 1.01)	8.5 ± 1.6 (2SD)
Inheritance (BD39)	553–2476 Ma (n = 6)	−56.6 to −14.6 (n = 5)	6.9 ± 1.8 (2SD)
Biotite-rich enclave (BD94) magmatic zircons	17.7 ± 0.2 Ma (n = 27, MSWD = 0.58)	−10.4 ± 1.3 (n = 12, MSWD = 1.6)	NA
Inheritance (BD94)	963–3139 Ma (n = 5)	−52.3 to −24.8 (n = 3)	NA

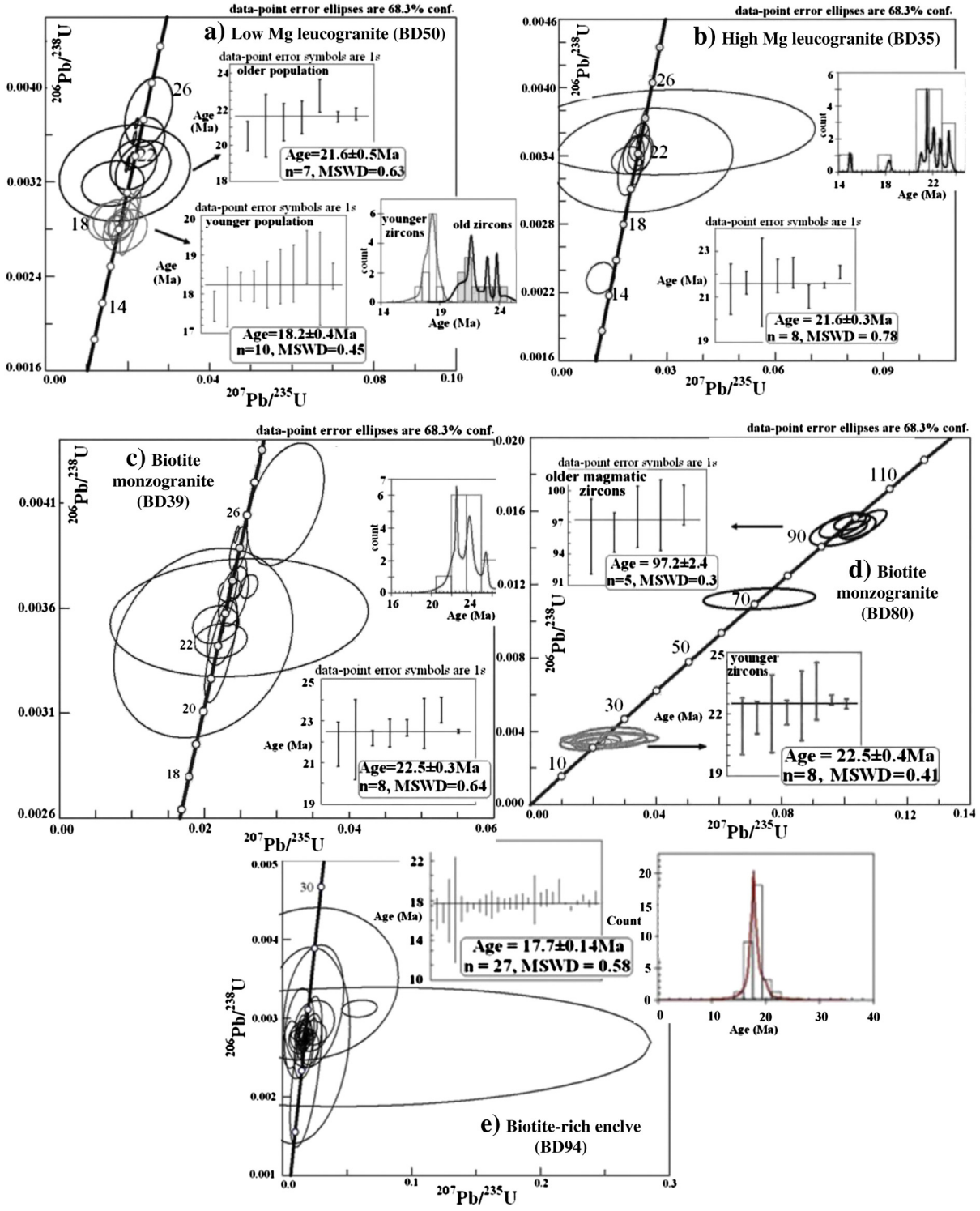

Fig. 4. U–Pb concordia plots and weighted mean ages of the Baltoro granites, a) low Mg leucogranite (BD50), b) high Mg leucogranite (BD35), c) biotite monzogranite (BD39), d) biotite monzogranite (BD80) and e) biotite-rich enclave (BD94) in monzogranite. Note that low Mg leucogranite also recorded a slightly younger age population at 18 Ma.

concentration of inherited cores is generally lower than in the Miocene overgrowth, ranging from 242 to 835 ppm corresponding to a lower U/Th ratio with a maximum of 10.6. Five inherited cores from the leucogranite BD35 yielded variable $^{206}Pb/^{207}Pb$ ages from 775 to 2504 Ma (Fig. 5b). Inherited cores are at less than 10% discordance except one strongly discordant core BD35-26 (1229 Ma). Six inherited cores from the monzogranite sample BD39 yielded ages of 553 to 2476 Ma (Fig. 5c). Two inherited cores are at less than 10% discordant, one is at <20% discordant while one sample (BD39-14) yielded age of 1026 ± 23 Ma with reverse discordance (103%). Biotite-rich enclave (BD94) rendered five inherited ages ranging from 963 to 3139 Ma. Three inherited cores yielded $^{206}Pb/^{207}Pb$ ages from 2473 Ma to 2486 Ma, one zircon yielded a younger age of 963 Ma while a euhedral zircon with oscillatory zoning yielded an age of 3139 ± 21 Ma (this is the oldest age among all the samples analyzed through this study) (Fig. 5d). All the cores are at less than 10% discordance. One analysis BD94-25 yielded an age of 78 ± 5 Ma.

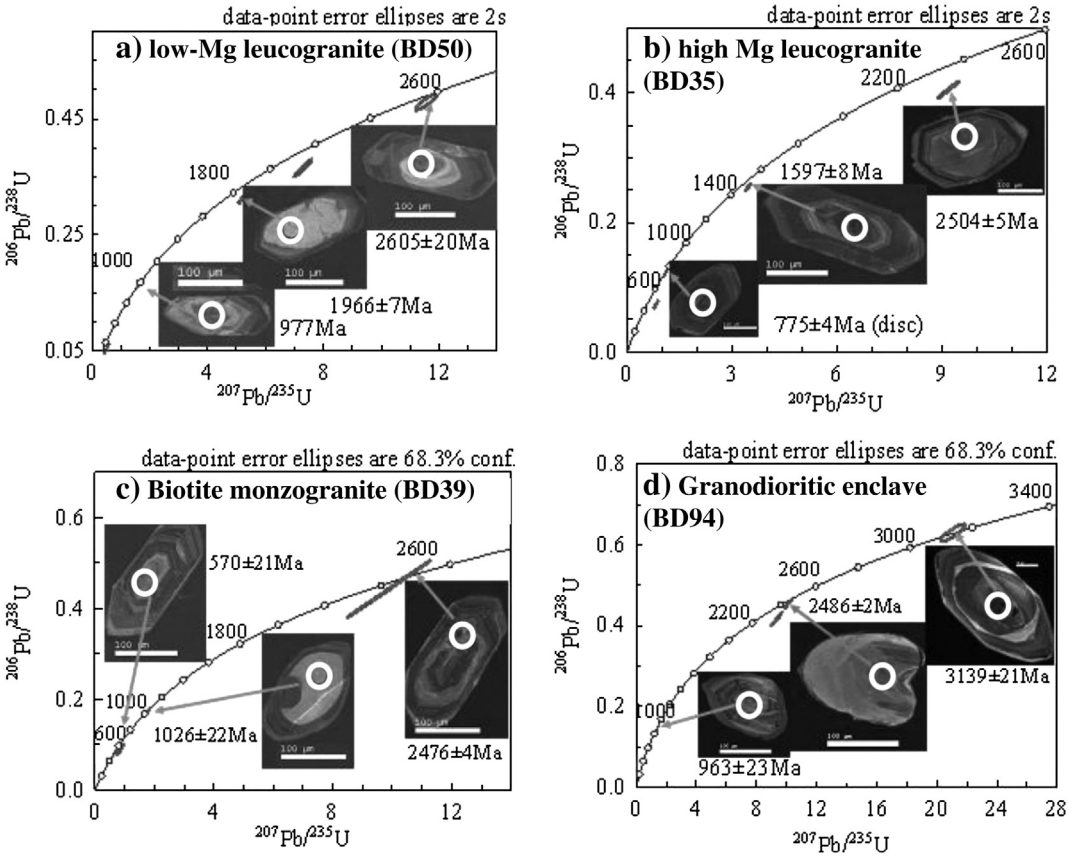

Fig. 5. U–Pb concordia plots showing inherited ages observed in a) low Mg leucogranite (BD50), b) high Mg leucogranite (BD35), c) monzogranite (BD39) and d) biotite-rich enclave (BD94).

4.2. Zircon Hf isotope data

4.2.1. Hf composition of magmatic zircons

Given the younger ages of magmatic zircons (26–15 Ma) and very little Hf in-growth (less than one epsilon unit), we report the present-day Hf isotope composition in terms of εHf (0) for the Neogene granites and biotite-rich enclave.

The weighted mean εHf values are presented at 95% confidence. Two leucogranite samples, BD50 and BD35 with indistinguishable WM age of 21.6 Ma yielded WM εHf (0) value of -8.1 ± 1.6 (MSWD $= 2.4$, n $= 8$) and -4.0 ± 0.9 (n $= 11$, MSWD $= 0.67$), respectively (Fig. 6a & b). The total range of Hf composition is -10.7 to -6.8 (BD50) and -6.1 to -2.4 (BD35). The younger population of zircons from BD50 with a WM age of 18.2 ± 0.4 Ma yielded a WM εHf (0) value of -8.1 ± 1.6 (MSWD $= 2.4$, n $= 8$) ranging from -10.9 to -4.9. Three analyses from high Mg leucogranite, BD35 presented more radiogenic composition with εHf (0) $= +1.7$ to $+4.4$ (BD35-23, 24 and BD35-36). BD35-24 is a homogeneous bright core showing evidence of dissolution while BD35-23 is the 15 Ma overgrowth surrounding the BD35-24 core, and is slightly more radiogenic than this core. BD35-36 is a thick homogeneous magmatic core, with strong oscillatory zoning and shows the highest radiogenic value of εHf (0) $= +4.4$. Two samples (BD50-31a and BD35-29) yielded extreme non-radiogenic εHf (0) value of -17.1 and -21.6 respectively and are not included in WM calculations.

Two biotite monzogranite samples, BD39 and BD80 with indistinguishable WM age of 22.5 Ma yielded WM εHf (0) of -4.5 ± 0.9 (MSWD $= 1.01$, n $= 9$) and -7.6 ± 1.0 (n $= 7$, MSWD $= 0.65$) respectively (Fig. 6c & d). The BD39 Hf composition is almost identical to the high Mg leucogranite (BD35) while BD80 rendered 3.1 ε-units lower than BD39 zircons of same age. Two spots on BD39 zircons show extreme values from non-radiogenic (BD39-33, εHf (0) $=-15.6$) to higher (BD39-13, εHf (0) $= +0.8$) Hf composition.

Six analyses on older (99 to 72 Ma) magmatic zircons yielded a present-day WM εHf (0) $= +0.9 \pm 1.0$ (n $= 6$, MSWD $= 1.13$) (Fig. 6e). Four analyses on zircons with $^{206}Pb/^{238}U$ ages of 96–99 Ma yielded radiogenic composition ranging from -0.4 to $+2.5$. One rim with a $^{206}Pb/^{238}U$ age of 72 Ma around a 96 Ma core showed slightly lower composition of -0.7. Another analysis in the same growth domain yielded the Hf composition of $+0.8$.

The biotite rich enclave with the WM age of 17.7 ± 0.14 Ma yielded the most non-radiogenic Hf signature with WM εHf (0) $= -10.4 \pm 1.3$ (n $= 12$, MSWD $= 1.6$) (Fig. 6f). One analysis with extreme non-radiogenic composition of εHf (0) $= -16$ is not included in the calculation, although the other 12 analyses also show variable Hf composition ranges from -14.4 to -7.3. However, out of the twelve, 9 analyses vary from -8.5 to -11.3.

4.2.2. Hf composition of inherited zircons

The initial εHf (t) for five inherited cores from low Mg leucogranite (BD50) with $^{206}Pb/^{207}Pb$ ages of 921 to 2605 Ma is variable ranging from -24.3 to -1.1. The projected present-day εHf (0) is non-radiogenic ranging from -58.6 to -21.4 (Fig. 7a). Note that the present-day Hf isotopic composition of inherited cores is significantly higher than in the Neogene magmatic zircons.

Inherited cores from high Mg leucogranite (BD35) of variable $^{206}Pb/^{207}Pb$ ages (812–2505 Ma) show highly variable heterogeneous initial εHf (t) from being highly radiogenic (sample BD35-3, εHf (1597 Ma) $= +10.6$) to non-radiogenic (sample BD35-26, εHf (1229 Ma) $= -15$). BD35-3 is a magmatic inherited core with strong

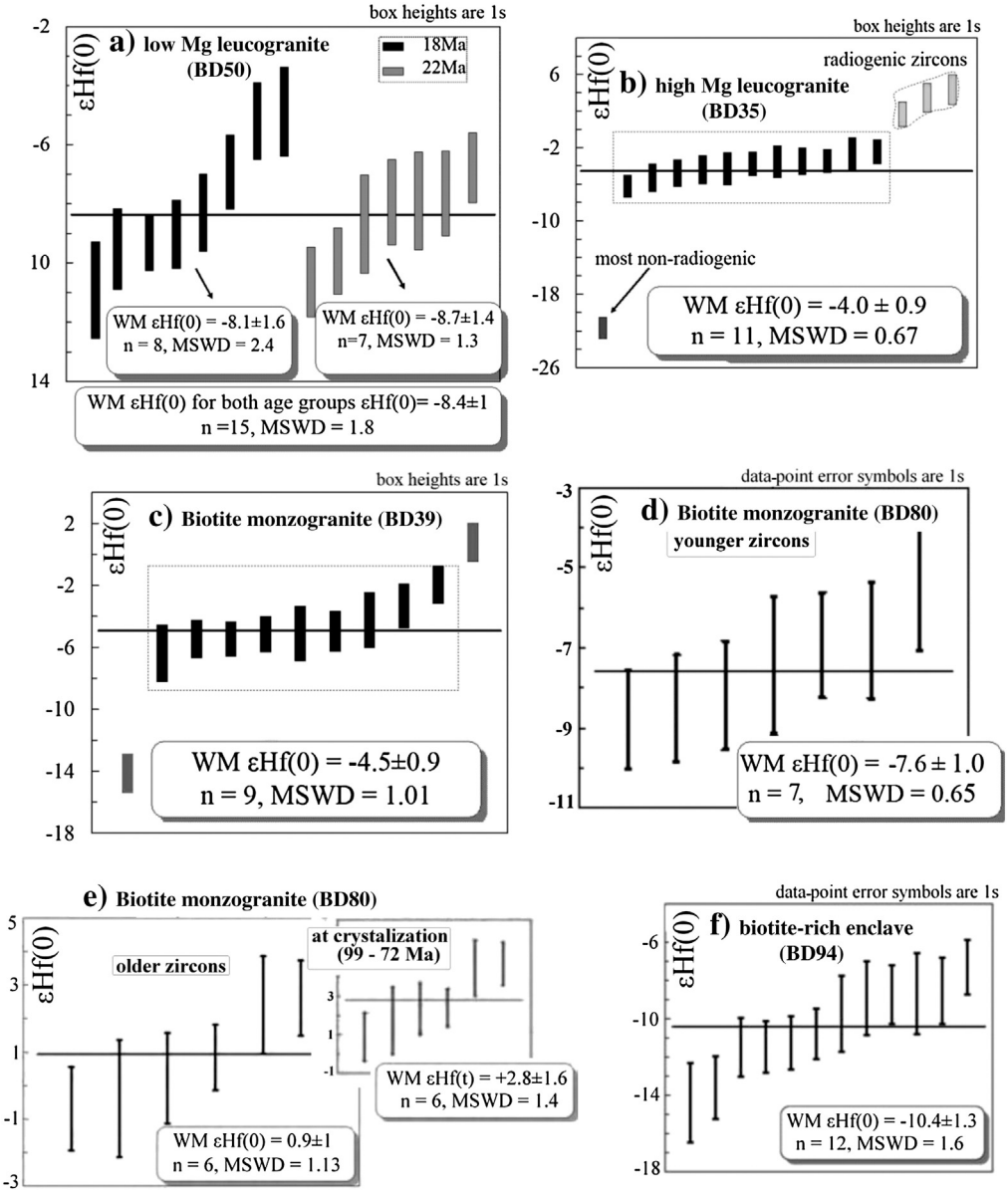

Fig. 6. Present-day weighted mean zircon Hf isotopic composition of Baltoro Plutonic Unit. a) Low Mg leucogranite (BD50), b) high Mg leucogranite (BD35), c) biotite monzogranite (BD39), d and e) biotite monzogranite (BD80), f) biotite-rich enclave (BD94). Some highly non-radiogenic and less evolved analyses are excluded from the weighted mean calculations.

oscillatory zoning while BD35-26 is a rounded, core surrounded by an oscillatory zoned rim. BD35-34, another homogeneous bright rounded core with no zoning visible shows εHf (2504 Ma) = +2.5. The present-day εHf (0) for five inherited cores vary from −53.9 to −22.5 (Fig. 7b).

Five inherited cores from BD39 with variable $^{206}Pb/^{207}Pb$ ages (553–2476 Ma) yielded complex and variable initial εHf (t) composition from being non-radiogenic that is −15.6 (BD39-12) to strongly radiogenic with εHf (t) value of +8.4 (BD39-30). The present-day Hf composition varies from εHf (0) −27.5 to −14.6 for the zircons with $^{206}Pb/^{207}Pb$ age ranging from 553 to 1059 Ma and one very old inherited core (2476 Ma) yielded εHf (0) of −56.6 (Fig. 7c).

Two oldest inherited cores in biotite rich enclave (BD94-18, 17) dated at 2484 and 2486 Ma yielded initial εHf (t) of +4.5 and +3.0 respectively, while another inherited core (BD94-19) (963 Ma) show mildly none-radiogenic composition of −3.9. The present-day εHf (0) for the oldest cores are −51.2 (BD94-18) and −52.3 (BD94-17). Inherited core BD94-19 rendered present-day εHf (0) of −24.8 (Fig. 7d).

4.3. Oxygen isotopic data

4.3.1. Oxygen isotopic composition of magmatic zircons

The oxygen isotopic composition of all Miocene zircons is homogenous. The oxygen isotopic value ($\delta^{18}O$) of both older (22 Ma) and younger (18 Ma) zircon populations from low Mg leucogranite (BD50) varies from 7.3 to 9‰. However four analyses yielded higher values ranging from 9.9–10.3‰. The oldest magmatic population (22 Ma) yielded a mean $\delta^{18}O = 8.4 \pm 1.4$‰ (n = 11, 2σ). While the youngest population (18 Ma) rendered slightly higher mean $\delta^{18}O$ of 9.4 ± 1.0‰ (n = 12) (Fig. 8a). The high Mg leucogranite (BD35) oxygen isotopic composition of magmatic zircons (21.6 ± 0.3 Ma) is homogeneous and varies from 8.3 to 9.5‰ with a mean of $\delta^{18}O = 8.9 \pm 0.7$‰ (Fig. 8b). These values

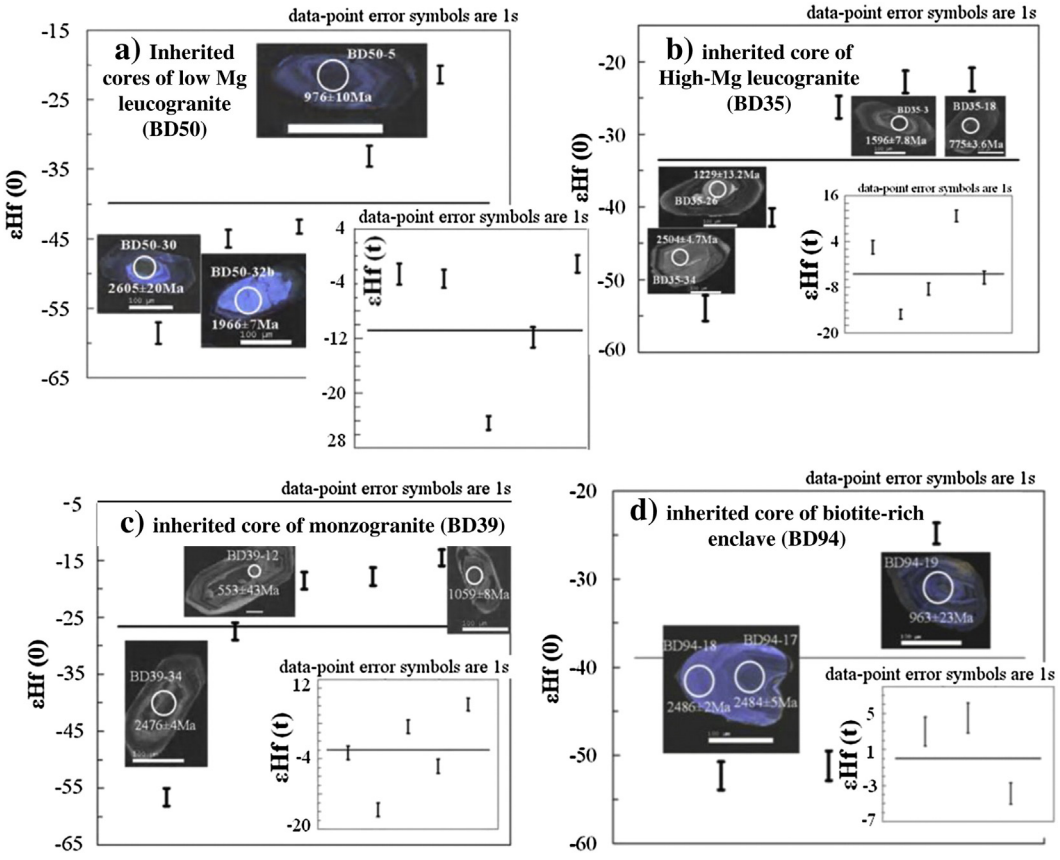

Fig. 7. Initial and present-day Hf composition of inherited core. a) Low Mg leucogranite (BD50), b) high Mg leucogranite (BD35), c) biotite monzogranite (BD39) and d) biotite-rich enclave (BD94).

are similar and undistinguishable from the low Mg leucogranite zircons (BD50).

The magmatic zircons (23 Ma) from two biotite monzogranites BD39 and BD80 show slightly lower but similar oxygen composition to the leucogranites. Their oxygen composition varies from 7.7 to 9.8‰. The mean $\delta^{18}O$ of BD 39 and BD80 is 8.5 ± 1.6‰ and 7.8 ± 0.4‰, respectively (Fig. 8c & d). Only one zircon BD39-3 yielded a lower value of 5.2‰. Two Cretaceous zircons (97 ± 2.4 Ma) from the monzogranite BD80 yielded the lowest mean oxygen composition of 7.7 ± 0.7‰. These values are however indistinguishable from the younger Miocene zircon population.

4.3.2. Oxygen composition of inherited core

Oxygen isotopic composition of the inherited core is relatively more variable. Inherited cores from the low Mg leucogranite (BD50) yielded a mean $\delta^{18}O$ of 8.1 ± 3.2‰, varying from 7.6 to 9.9‰, only two cores (BD50-5 and BD50-7) show lower juvenile values of 6.4 and 5.3‰ respectively (Fig. 8a).

Inherited cores from high Mg leucogranite sample (BD35) present variable oxygen compositions ranging from 8.3 to 9.3‰. Higher $\delta^{18}O$ values of 10.7 and 11.3‰ were obtained from two rounded bright cores BD35-5 and BD35-26, respectively. Three cores BD35-3, BD35-17 and BD35-27 are juvenile in terms of their oxygen composition (Fig. 8b). BD35-3 inherited core (1597 Ma) also shows higher εHf (t) of +10.6 supporting its juvenile character.

Inherited cores from monzogranite BD39 present relatively homogeneous lower oxygen composition with mean $\delta^{18}O$ = 6.9 ± 1.8‰. Six out of ten cores yielded $\delta^{18}O$ value ranging from 5.5 to 7.4‰ and two zircons rendered value of 8.1‰. Only one bright rounded homogeneous core (BD39-14) with no visible zoning present higher value of 9.9‰ (Fig. 8c).

5. Discussion

5.1. Timing of magmatism in the Baltoro plutonic unit

5.1.1. Miocene magmatism

Our new U–Pb ages (26–15 Ma) largely corroborate earlier ages reported for Baltoro granites (e.g., Parrish and Tirrul, 1989; Schärer et al., 1990; Searle et al., 2010). The two age populations suggest two zircon crystallization episodes, one around 18 Ma and one at 21–23 Ma. The youngest ages (15–18 Ma) are only observed in leucogranites as well as in the biotite-rich enclave. However, 21 to 23 Ma ages were observed in all granitic samples. The majority of the younger zircon ages (≤18 Ma) is from the rims around older magmatic zircons (i.e., ~22 Ma population). All zircons show similar, low (U/Th) ratio indicative of an igneous origin. Slightly higher $\delta^{18}O$ values in the younger zircons from the low Mg leucogranite (BD50) indicate interaction of the partial melt generated in the lower crust with a metasedimentary source at shallow depths, possibly during the ascent and final emplacement of the magma.

The biotite-rich enclave (BD94) within biotite monzogranite, provide U–Pb ages indistinguishable from the 18 Ma event recorded in BD50. Few ~18 Ma zircons from BD50 yielded comparable Hf composition to the BD94. This suggests that the second crystallization event recorded in the low Mg leucogranite (BD50) could be related to later injection of a source similar to the biotite-rich enclave (BD94). Based on its mineralogical features (biotite and amphibole rich), sample BD94 is most probably related with mantle melt and could be a plutonic equivalent of the lamprophyre emplaced at 22–24 Ma (Rex et al., 1988).

This is supported by the similar whole rock Hf isotopic value of a Baltoro lamprophyre (εHf (0) = −9.3; Mahéo et al., 2009) to the BD94 zircon values. Lamprophyre was also emplaced at 24 Ma near

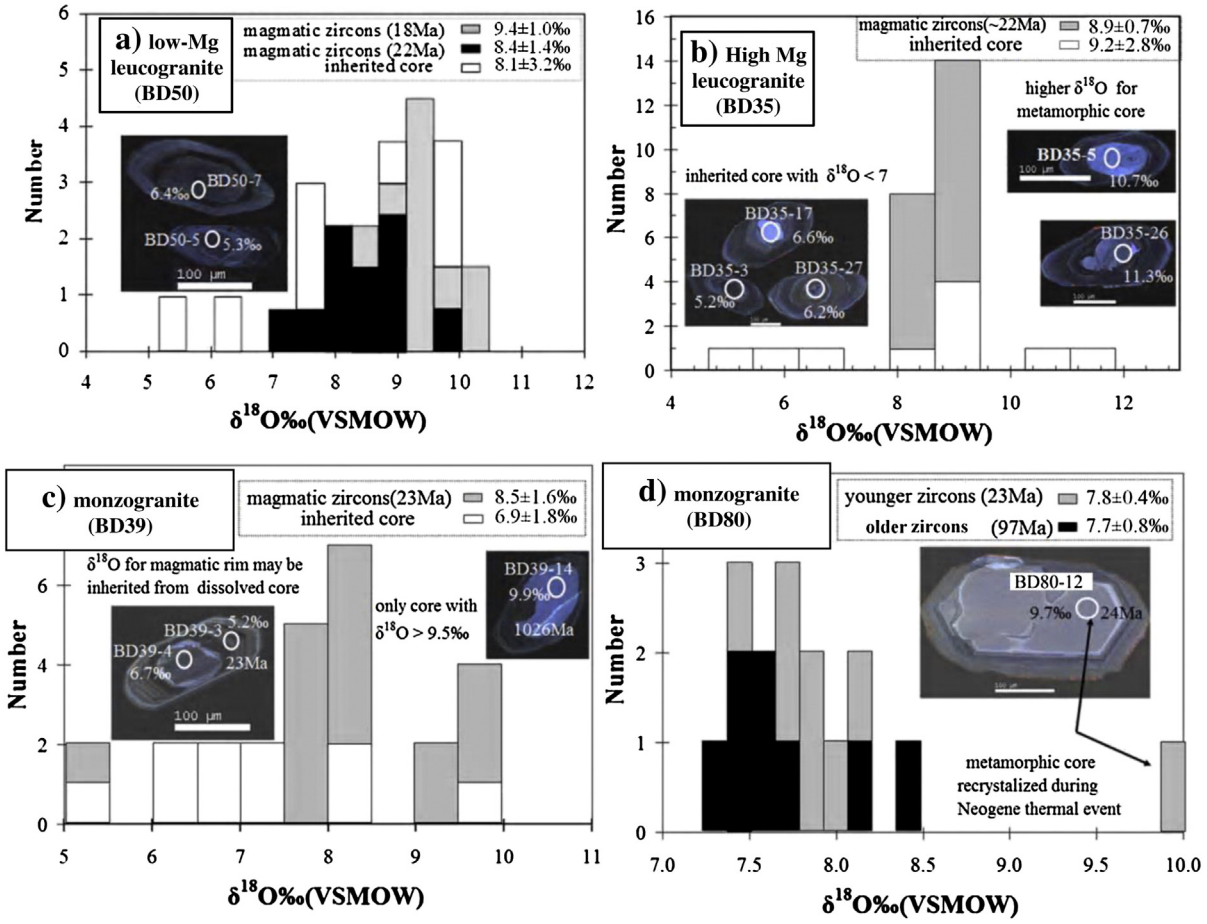

Fig. 8. Histogram of individual oxygen isotope analyses. (a) Low Mg leucogranite (BD50), b) high Mg leucogranite (BD35), c) biotite monzogranite (BD39), d) biotite monzogranite (BD80). Majority of the Miocene magmatic zircons showed indistinguishable oxygen composition ranges from 7 to 9.5‰. Few inherited cores showed juvenile oxygen composition (~5 to 6.5‰). VSMOW: Vienna Standard Mean Ocean Water.

Leh, intruding the Ladakh batholith (Ravikant, 2006). Intrusion of 22–24 Ma lamprophyre and analogous U–Pb ages (i.e., 22–23 Ma) of Baltoro granites is consistent with the interpretation that the Baltoro granite emplacement was contemporaneous with mantle melting. Also the U–Pb zircon crystallization ages suggest that the onset of melting associated with the Baltoro emplacement took place sometime before crystallization of the oldest magmatic zircon at ~24 Ma and that coincides with the intrusion of 22–24 Ma lamprophyre suggesting that a melting event occurred around 24 Ma. The second zircon crystallization event at ~18 Ma is related to a secondary magma injection that should have taken place sometime before 18 Ma and after the crystallization of the first zircon population (21–23 Ma). Additionally, this secondary injection may have originated from a magma stored at depth and related with a melting episode significantly older than the injection age. Consequently, two melting events are not required to explain the two zircon crystallization episodes.

5.1.2. Early–Middle Cretaceous ages from Baltoro granites

In south Karakoram, Cretaceous magmatism (~85–130 Ma) has been previously recognized in several studies (e.g., Fraser et al., 2001; Heuberger et al., 2007; Le Fort et al., 1983; Searle et al., 1999). This magmatic event is related to the convergence between the Kohistan arc and the south Karakoram active margin during the closure of the Shyok back-arc resulting in the formation of the Shyok suture zone at ~75–80 Ma (see Searle et al., 1999 for review). The southwestern Karakoram Cretaceous (121–104 Ma) rocks (granites, diorites and a basalt sill) in the southern Chitral (next to the suture with the Kohistan) yielded initial εHf (t) ranging from −1.8, +3.4 to +10.9 while the older zircons yielded the values of −4.8 to +3.9 (Heuberger et al., 2007). These Hf values were interpreted as continental arc magmatism with a clear indication of Cretaceous subduction beneath the Karakoram terrane. The variable initial Hf (t) values suggest varying melt composition between a crustal end member and a depleted (MORB-type) mantle that is consistent with a continental margin setting (Heuberger et al., 2007).

Early Cretaceous zircons (97–72 Ma) in monzogranite BD80 yielded the most radiogenic Hf composition of this study with εHf (0) ranging from −0.7 to +2.5. These values are indistinguishable from Karakoram calc-alkaline (south Chitral) and Mesozoic Karakoram batholiths (Pangong Range in east). Thus, age as well as Hf isotopic ratio suggests that BD80 zircons could be entrained from the early Cretaceous calc-alkaline basement beneath south Karakoram. This interpretation is compatible with previous Nd and Sr isotopic as well as whole rock chemistry characteristics of the Baltoro granites that suggest that this latter derived from the melting of a subduction-related dioritic or granodioritic crust (Mahéo et al., 2009). Similar granites (ASI or A/CNK ~0.9–1.1; Fig. 2c), called peraluminous I-type granites (Chappell et al., 2012; Clemens et al., 2011; Petford and Atherton, 1996), have been associated with dioritic or granodioritic source melting. Experimental studies on various basic sources imply that the melting is controlled by biotite or amphibole dehydration melting reactions (Beard and Lofgren, 1991; Beard et al., 2005; Petford and Atherton, 1996; Rapp

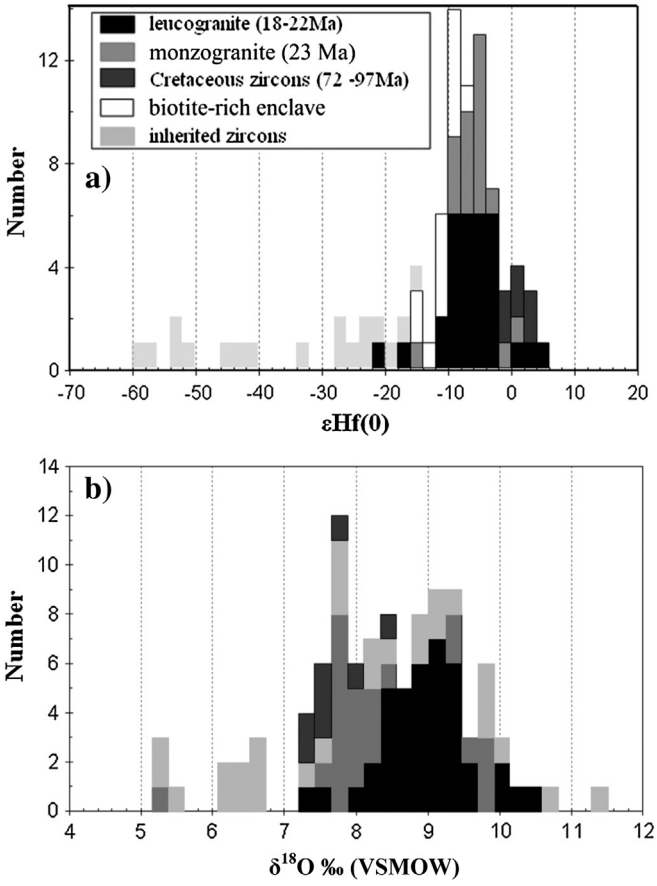

Fig. 9. Overall variations in (a) εHf (0) and (b) $\delta^{18}O$. Frequency histograms based on all the studied zircons.

and Watson, 1995; Sen and Dunn, 1994; Vielzeuf and Schmidt, 2001) at a temperature of about 850–950 °C.

5.1.3. Zircon inheritance

Zircon inherited ages (n = 22) are variable, ranging through the entire Proterozoic (553–3139 Ma). These ages are consistent with those

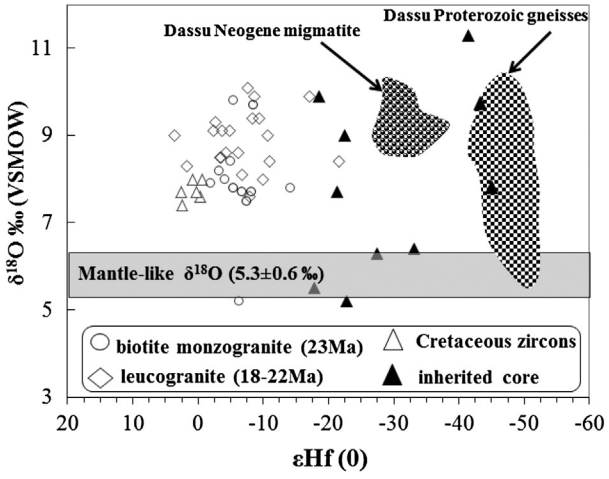

Fig. 10. Plot of $\delta^{18}O$ versus εHf (t) values for magmatic and inherited zircons. Note that except few inherited cores, none of the zircons showed mantle-like oxygen composition. Fields of the south Karakoram Dassu Neogene migmatites and Proterozoic inherited core are from Mahar et al. (submitted for publication). Mantle-like oxygen composition is from Valley et al. (2005).

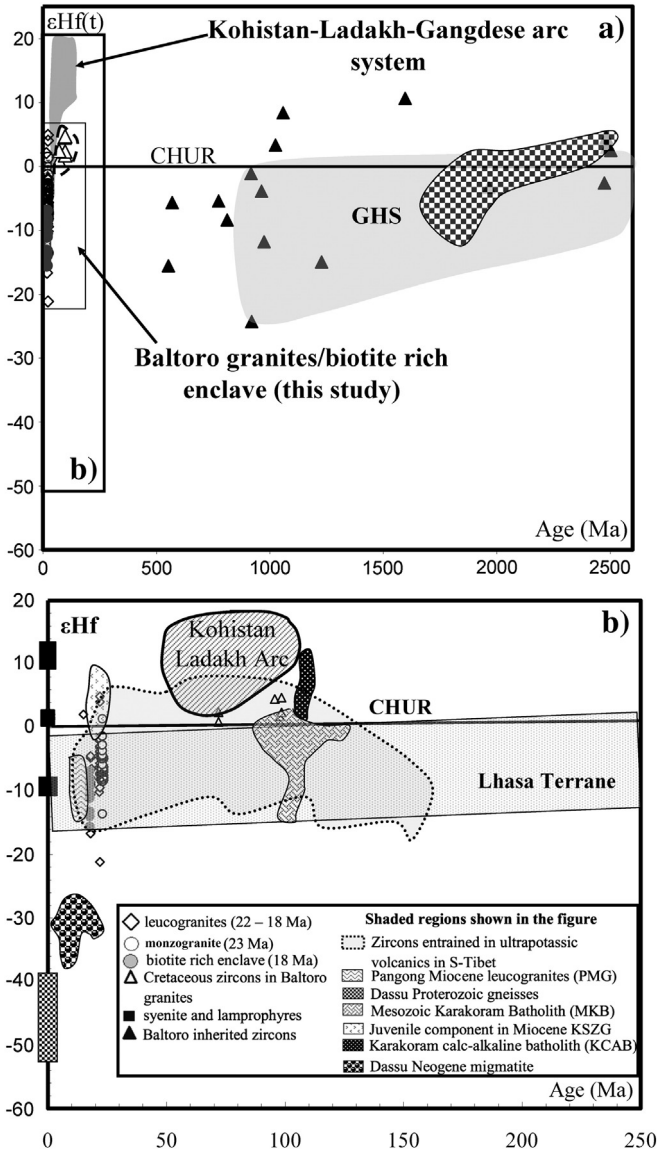

Fig. 11. (a) Evolution of Hf isotopic composition with time and comparison with spatially and temporally related lithotectonic units. (b) Represents the rectangle shown in (a). Shaded regions: (1) Ladakh/Kohistan batholith (Bouilhol et al., 2011, 2013; Heuberger et al., 2007; Ravikant et al., 2009; Schaltegger et al., 2002), Gangdese batholith (Chiu et al., 2009; Chu et al., 2006; Wu et al., 2007), (2) Indian crust (Greater Himalayan Sequence [GHS] (Richards et al., 2005), (3) juvenile component of Karakoram Shear Zone leucogranites (KSZG) (Horton and Leech, 2013; Ravikant et al., 2009), (4) Karakoram Cretaceous calk-alkaline batholith (KCAB) (Heuberger et al., 2007), (5) Mesozoic Karakoram Batholith (MKB in eastern Karakoram) (Ravikant et al., 2009), (6) Pangong Miocene granites (PMG) (Horton and Leech, 2013; Ravikant et al., 2009), (7) south Tibet, Lhasa terrane (Chu et al., 2006; Wu et al., 2007; Zhang et al., 2007), (8) Dassu and Baltoro lamprophyre/syenite (Mahéo et al., 2009), (9) xenocrystic zircons from the ultapotassic volcanics in south Tibet Lhasa terrane (Liu et al., 2014), (10) Dassu Neogene migmatites and Proterozoic inherited core (Mahar et al., submitted for publication).

reported from the Lhasa block in south Tibet (Chiu et al., 2009; Leier et al., 2007). This supports the Gondwana affinity of the Karakoram terrane, a westward continuation of south Tibet (Lhasa block).

Mixed oxygen composition (5.2 to 11.3‰) and variable present-day Hf composition (−58.6 to −14.6) (Figs. 8–10) indicates that the inherited cores of variable ages were sourced from different materials. Some appear to be juvenile while others are crystallized from a melt generated by melting of supracrustal rocks. However our data do not constrain the exact sources for inherited zircons. These values are comparable with the Proterozoic gneisses and Neogene migmatites of

Karakoram metamorphic complex in the Dassu area (data shown in Figs. 10 & 11; Mahar et al., submitted for publication).

5.2. Hf and oxygen isotopic variations in the Baltoro granites

Fig. 9a & b shows the overall variation and spread of the Hf and oxygen isotopic compositions, respectively. Baltoro Plutonic Unit show heterogeneous Hf composition ranging from εHf (0) = −17.1 to +4.4 (Fig. 9a). These values are significantly higher than the south Karakoram migmatitic gneisses with indistinguishable oxygen composition of ~7 to 9.5‰ (Fig. 10). Except few inherited cores, none of the zircons fall in the mantle-like oxygen composition of 5.3 ± 0.6‰ (Valley et al., 2005) (Figs. 9b & 10).

We plotted the observed Hf composition of the Baltoro zircons with spatially related lithotectonic units (Fig. 11). The observed Hf isotopic composition of granites is broadly similar to the previously reported whole rock Hf isotopic data from these rocks (Mahéo et al., 2009). Our new Hf data are comparable to the zircon Hf composition of the granites from the Lhasa terrane in south Tibet (Chu et al., 2006; Wu et al., 2007; Zhang et al., 2007). Recently, Liu et al. (2014) presented the U–Pb ages and Hf isotopic composition of the xenocrystic zircons entrained in the ultrapotassic volcanic rocks in southern Tibet. They identified three magmatic pulses at 90, 50 and 20 Ma. These subduction related (90 Ma), syn-collisional (50 Ma) and post thickening (20 Ma) magmatic episodes coincides with the magmatic rocks in the south Karakoram (e.g., Mahéo et al., 2009; Searle et al., 2010). The Hf composition of these xenocrystic entrained zircons is heterogeneous and indistinguishable from the Miocene Baltoro granites, Pangong Range leucogranites and Mesozoic Karakoram batholith (Fig. 11b). This strengthens the interpretations emphasizing the genetic link between the Karakoram and south Tibet.

For comparison, Hf data from the juvenile Kohistan–Ladakh Gangdese arc system are also shown (Fig. 11a & b). The Hf compositions observed in the Baltoro granites are intermediate between the inherited zircons observed from the migmatitic gneisses in the south Karakoram (Mahar et al., submitted for publication) and Cretaceous calc-alkaline granodioritic lithologies of Karakoram terrane (Figs. 10 & 11b). Therefore, mixing is inferred between Cretaceous calc-alkaline magmatic rocks either with the old Karakoram crust and/or with the metamorphic rocks in south Karakoram. If zircon εHf (0) is plotted against $^{206}Pb^*/^{207}Pb$ (Fig. 12), a more complex origin is evident. The observed Baltoro isotopic characteristics are better explained if three sources are involved (1) Cretaceous calc-alkaline Karakoram crust, (2) Karakoram gneisses, and (3) a third source which mostly influences BD94 isotopic composition. As this latter has a mafic mineralogy (biotite, amphiboles) with εHf values similar to the Karakoram lamprophyres (Mahéo et al., 2009), it is suggested that the third source is the Asian lithospheric mantle. Involvement of mantle melts in the south Karakoram Miocene magmatism is required by the presence of lamprophyre (Mahéo et al., 2002; Searle et al., 1992). Based on Sr, Hf and Nd isotopic composition of the lamprophyre, Mahéo et al. (2009) suggested that their mantle source has been metasomatised by fluid released by the subduction of Indian continental margin. However, our data do not allow us to evaluate this hypothesis further.

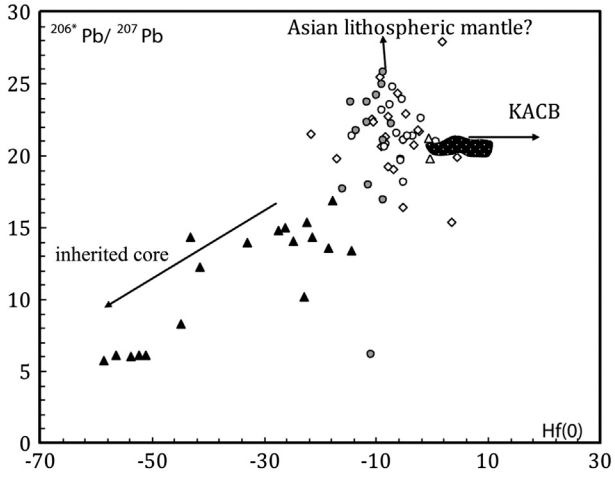

Fig. 12. Plot of zircon εHf (0) versus $^{206}Pb^*/^{207}Pb$ (ratio) for the Baltoro samples, and south Karakoram calc-alkaline rocks (Heuberger et al., 2007). Same symbols as in Fig. 11.

The homogenous oxygen composition of Baltoro granites (~7 to 9.5‰) is 1–2.5‰ heavier than the typical igneous zircons at high temperature (~7‰, Valley, 2003). This may have resulted from interaction with the metasomatised Asian mantle or mid-crustal migmatitic gneisses at relatively lower temperature. Whole rock oxygen isotopic composition of younger leucogranites from the Karakoram batholith is 1 to 2‰ higher than our Neogene zircons, ranging from 9.5 to 10.7‰. Oxygen composition of Cretaceous zircons (97–72 Ma) (7 to 8‰) are comparable with the whole rock oxygen composition obtained from the Cretaceous granodiorites of the Karakoram batholith that is 6.2 to 7.7‰ (Srimal et al., 1987) (Figs. 9b & 10). These oxygen values are consistent with the interpretation that the zircons crystallized from a magma generated by melting of pre-existing igneous rocks mixed with evolved sources at the lower–middle crust. No evidence has been observed for direct contribution of pristine mantle derived magmas as none of the zircons yielded mantle type oxygen composition (5.3 ± 0.6‰, Valley et al., 2005) (Fig. 10).

Thus, our data are not consistent with the supra-crustal origin alone for Baltoro granites that was proposed by Schärer et al. (1990) based on zircon and monazite inheritance and whole rock isotopic data (Pb, Sr and Nd). They proposed the meta-sedimentary rocks of Karakoram Metamorphic Complex (KMC) were the dominant source for the Baltoro granites. Instead, our data suggest more complex hybridization between infra and supracrustal components in the Baltoro Neogene magmatism.

Proterozoic gneisses (1.8–1.9 Ga) and Neogene migmatites (20–5.9 Ma) in the KMC have highly non-radiogenic Hf compositions with εHf (0) ranging from −50 to −30 which is significantly lower than the Baltoro granites (Mahar et al., submitted for publication; Figs. 10 & 11b). Therefore, partial melting of Karakoram Proterozoic gneisses present at the midcrustal depths alone would not be able to produce the batholith sized Baltoro granites by simple mica dehydration melting reactions. The mildly peraluminous alkali-calcic to calc-alkaline composition, lack of tourmaline and higher temperature of granites is not consistent with the extensive melting of metapelites at relatively lower temperature. If similar rocks from the Karakoram Metamorphic Complex would have been the only source for the Baltoro granites then the Hf composition observed in the Baltoro region should have more non-radiogenic compositions around −20 to −30. Nevertheless, some lower values (<−10) coupled with increased oxygen composition (>7‰), indicates a contribution from relatively evolved sources; either from the old non-radiogenic Karakoram crust (Ordovician–Precambrian) or the Karakoram metamorphic rocks farther south.

The contemporaneous mafic sample (BD94) presents relatively non-radiogenic Hf composition (εHf (0) = −10.4) similar to the Baltoro lamprophyre (εHf (0) = −9.3, Mahéo et al., 2009). Such composition is very different from Cretaceous mafic rocks studied in south Karakoram with generally positive εHf (0) (Heuberger et al., 2007; Ravikant et al., 2009; Schaltegger et al., 2002). This suggests either that Neogene and Cretaceous mafic rocks derived from a different mantle source or that the mantle isotopic composition evolved through time. Mahéo et al. (2009) and Ravikant et al. (2009) proposed that the non-radiogenic values from Neogene south Karakoram magmatic rocks derived from a contribution of the subducted Indian crust. This latter could modify the south Karakoram mantle isotopic composition through fluid transfer (Mahéo et al., 2009).

5.3. Relationship of Baltoro granites with Pangong Range and western Tibet magmatic rocks

Based on previous geochronological, geochemical and isotopic data (mainly Sr and Nd and Hf) from Baltoro granites (Crawford and Windley, 1990; Mahéo et al., 2002, 2009; Searle et al., 1992) and from Pangong Range/Karakoram batholith (Boutonnet et al., 2012; Horton and Leech, 2013; Ravikant et al., 2009; Reichardt et al., 2010; Searle and Phillips, 2007; Searle et al., 1998), a genetic link has been proposed for the Neogene magmatic activity in the Baltoro plutonic unit and its possible eastward continuity within the Karakoram fault zone (Karakoram Shear Zone, KSZ) and in the Karakoram batholith; i.e. leucogranites exposed in the Pangong Range and Nubra valley (Fig. 1). In the Karakoram shear zone two groups of granitoids have been recognized (i) calc-alkaline foliated granite and granodiorites emplaced between 55 and 74 Ma and (ii) leucogranites mostly emplaced around 17–19 Ma with latest stage at about 14 Ma (see Boutonnet et al., 2012; Horton and Leech, 2013 for review). The timing of emplacement and εHf (t) values (Fig. 11b), confirm the correlation between the Baltoro and the Miocene rocks deformed in the Pangong Range. However, Horton and Leech (2013) and Ravikant et al. (2009) also reported juvenile, εHf (t) values (+1 to +9) from Karakoram Shear Zone leucogranites, a significant contribution either from less evolved Karakoram Cretaceous calc-alkaline and/or juvenile adjacent Ladakh batholith. Using zircon Hf isotope compositions, the Baltoro granite can be correlated with the Miocene Karakoram batholith (Fig. 1) that is also connected with the Pangong Range (Reichardt et al., 2010). We conclude that the Baltoro, Pangong Range and Miocene Karakoram batholith belong to the same magmatic event related with partial melting of pre-existing calc-alkaline, Cretaceous plutonic rocks of the Karakoram terrane. Contamination by metamorphic rocks is also evident in all three areas (Ravikant et al., 2009; Reichardt et al., 2010). Farther south, this Miocene plutonic zone is characterized by ultrapotassic volcanic rocks (Fig. 1; Shiquanhe area) emplaced between 18 and 24 Ma (Arnaud et al., 1992; Williams et al., 2004). These rocks belong to the south Tibetan Miocene, potassic belt (Miller et al., 1999; Turner et al., 1996). The Shiquanhe Miocene rocks are contemporaneous with the emplacement of the Baltoro and associated lamprophyres and share the same Sr and Nd isotopic composition to the magmatism in the Baltoro region (Mahéo et al., 2009; Searle et al., 1992). This suggests that both the Baltoro and Shiquanhe Miocene volcanics are emplaced from a similar source and during the same magmatic event. This event implies both melting of a crustal source and of metasomatised Asian mantle (Mahéo et al., 2002, 2009; Williams et al., 2004).

The Baltoro, Pangong Range, Miocene Karakoram Batholith, and Shiquanhe volcanic rocks belong to the same magmatic belt. The shape of this belt and of the various outcrops (Fig. 1) suggests that this magmatic zone has been offset and stretched by Karakoram fault. Moreover, as the Karakoram fault was active since 26 Ma (see Leloup et al., 2011 for discussion), this latter (Karakoram fault) may have localized melt ascent and intrusion of plutonic rocks, especially in the transpressional Pangong Range.

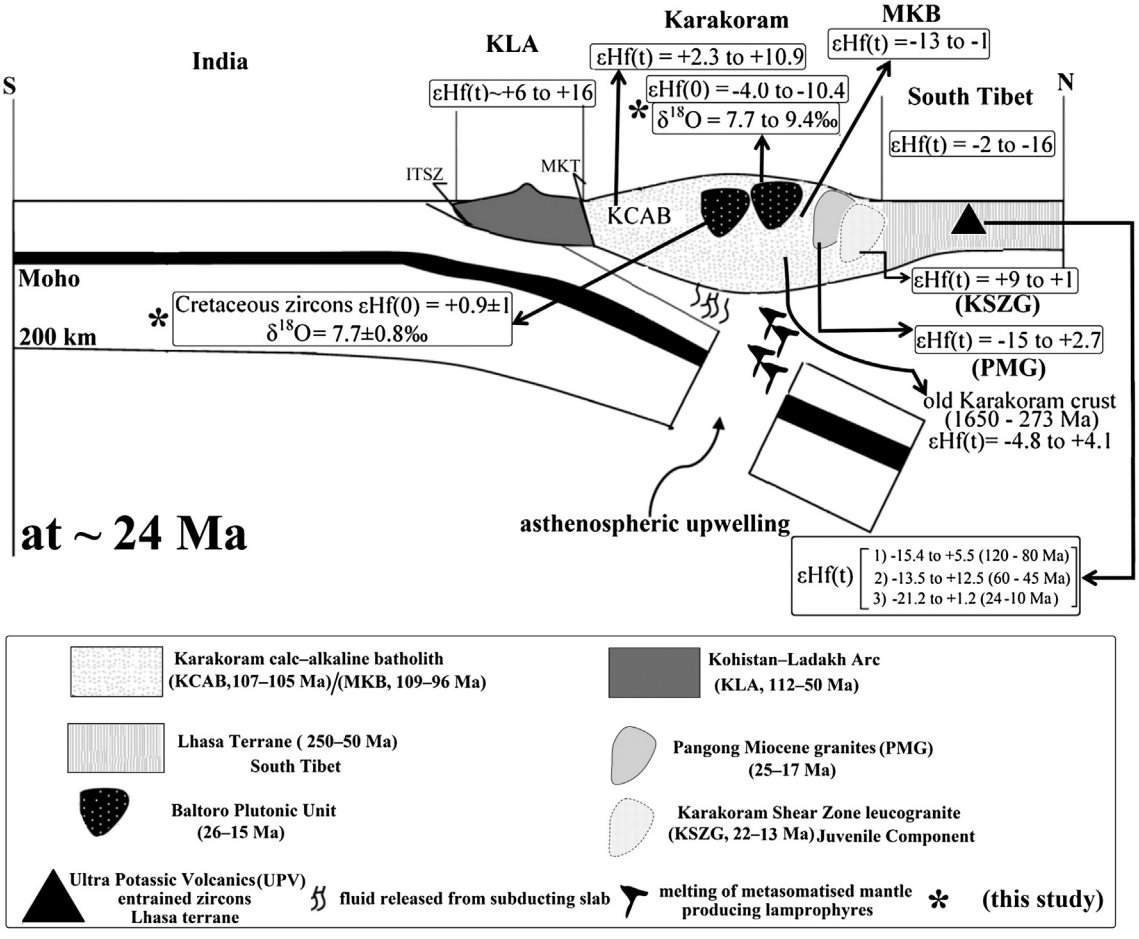

Fig. 13. Schematic tectonic configuration at 24 Ma following India–Asia collision. The abbreviations and Hf data used for related lithotectonic units are same as in Fig. 11.

5.4. Karakoram–South Tibet Geodynamics

This new study confirms that a significant magmatic event took place in south Karakoram between 18 and 23 Ma and that it can be associated with the Miocene south Tibet magmatism. Melting involved both crustal and mantle sources as evident by contemporaneous lamprophyre and associated rocks (such as BD94). Simple melting by thermal re-equilibration following crustal thickening as modeled by Thompson and Connolly (1995) cannot account for the mantle melt as well as the short duration of the melting event. In South Tibet, such bimodal magmatism was related either with mantle delamination (Chung et al., 2005), continental subduction (Ding et al., 2003) or detachment of the subducting Indian continental lithosphere (slab break-off, Chemenda et al., 2000; Williams et al., 2004). As previously discussed by Mahéo et al. (2009) mantle delamination, is incompatible with the location of the melting, following a narrow belt stretching from south Karakoram, Pangong Range to south Tibet, parallel with the India–Asia suture zone (Fig. 1). Such geometry is better explained by a slab-related process. Thus, following Mahéo et al. (2002, 2009), we propose that the Baltoro emplacement is related with the detachment of the subducting Indian continental lithosphere (Fig. 13). In south Karakoram and adjacent areas dating of ultrapotassic volcanic rocks suggest that mantle melt took place between ~18 and 24 Ma. Such short melting event is compatible with continental slab breakoff thermo-mechanical modeling that suggests a mantle melting duration of a few million years (Van de Zedde and Wortel, 2001). However, crustal melt crystallization took place as late as ~14 Ma in the Baltoro area (Searle et al., 2010) and ~9 Ma in the Pangong Range, Karakoram shear zone (Horton and Leech, 2013). This may either be related to late crystallization of an earlier melt during slow cooling or late melting promoted either by post thickening thermal re-equilibration of the previously thickened Karakoram crust, shear heating or adiabatic decompression along the Karakoram Fault.

In Fig. 13, we summarize the post collision plate configuration at ~24 Ma. Key to this interpretation is that our Hf–O data indicate that the melt source did not sample the juvenile Kohistan–Ladakh arc component; i.e., during Miocene time Kohistan-type arc related lithologies did not melt and this is evident by the absence of post ~35 Ma magmatism in Kohistan–Ladakh arc. The southern part of the Kohistan batholith is generally older than 95 Ma while younger ages up to 34 Ma were reported from the northern part of the batholith close to Kohistan–Karakoram suture zone (Bard, 1983; Coward et al., 1982; Heuberger et al., 2007; Jan and Howie, 1981; Schaltegger et al., 2002; Treloar et al., 1989). These ages from Kohistan batholith suggest that the youngest magmatic event lasted until Eocene (e.g., Heuberger et al., 2007). This has implications to the location of the breaking of Indian continental lithosphere and the angle of the subducting slab in the Miocene. We suggest that around 24 Ma cold continental slab had already passed beneath the Kohistan–Ladakh arc system with a significant part of the slab beneath the Karakoram terrane. Thus, during a slab breakoff event, heat advected by asthenospheric upwelling was not able to melt the Kohistan arc lithosphere which had been obducted onto the Indian continental margin. Instead, an asthenospheric window opened beneath the Karakoram lithosphere basement inducing its melting.

6. Conclusion

- The combined U–Pb, Hf and oxygen data demonstrate that the Baltoro granites were formed by partial melting of pre-existing igneous sources, mixing with old Karakoram basement and/or mid-crustal rocks of Karakoram metamorphic complex is likely. This is corroborated by previous interpretations emphasizing partial melting of mafic Karakoram lower crust at 26–21 Ma (Mahéo et al., 2009).
- The Early–Mid Cretaceous calc-alkaline basement in the Karakoram terrane with similar and relatively more heterogeneous isotopic composition is the potential source. Mixing of such magma either with the adjacent juvenile Kohistan–Ladakh batholith or pristine mantle derived magmas is less likely because our oxygen and Hf isotopic data do not show evidence of a juvenile component. Moreover, the Hf compositions observed in Kohistan–Ladakh arc are significantly more radiogenic (+6 to +16) than the Baltoro granites. However, contamination from metasomatised Asian mantle with modified O–Hf composition is suggested.

Supplementary data to this article can be found online at http://dx.doi.org/10.1016/j.lithos.2014.07.014.

Acknowledgments

We are grateful to Dominique Giesler, Mark Pecha and Dr. Clayton Loehn at LaserChron, University of Arizona for technical assistance in the sample preparation, analysis, and data reduction isotopic data (U–Pb and Hf) acquisition and zircon BSE & CL-imaging. The authors also thank Dr. Kouki Kitajima at WiscSIMS, UW-Madison for tuning and operation of the IMS-1280 instrument and assistance with sample preparation, analysis (oxygen isotopic measurements), and data reduction and interpretation. WiscSIMS is partly supported by NSF EAR1053466. F. Debon is thanked for providing the samples.

References

Andersen, T., Griffin, W.L., 2004. Lu–Hf and U–Pb isotope systematics of zircons from the Storgangen intrusion, Rogaland Intrusive Complex, SW Norway: implications for the composition and evolution of Precambrian lower crust in the Baltic Shield. Lithos 73, 271–288.

Appleby, S.K., 2008. The Origin and Evolution of Granites: An In-situ Study of Zircons from Scottish Caledonian Intrusions. Ph.D. Thesis University of Edinburgh.

Appleby, S.K., Gillespie, M.R., Graham, C.M., Hinton, R.W., Oliver, G.J.H., Kelly, N.M., EIMF, 2010. Do S-type granites commonly sample infracrustal sources? New results from an integrated O, U–Pb and Hf isotope study of zircon. Contributions to Mineralogy and Petrology 160, 115–132.

Arnaud, N.O., Vidal, P., Tapponier, P., Matte, P., Deng, W.M., 1992. The high K_2O volcanism of north western Tibet: geochemistry and tectonic implications. Earth and Planetary Science Letters 111, 351–367.

Bard, J.P., 1983. Metamorphism of an obducted island arc: example of the Kohistan sequence (Pakistan) in the Himalayan collided range. Earth and Planetary Science Letters 65, 133–144.

Beard, J.S., Lofgren, G.E., 1991. Dehydration melting and water-saturated melting of basaltic and andesitic greenstones and amphibolites at 1, 3, and 6.9 kb. Journal of Petrology 32, 365–401.

Beard, J.S., Ragland, P.C., Crawford, M.L., 2005. Reactive bulk assimilation: a model for crust–mantle mixing in silicic magmas. Geology 33, 681–684.

Belousova, E.A., Griffin, W.L., O'Reilly, S.Y., 2006. Zircon crystal morphology, trace element signatures and Hf isotope composition as a tool for petrogenetic modelling: examples from eastern Australian granitoids. Journal of Petrology 47, 329–353.

Bertrand, M., Debon, F., 1986. Evolution tectonique polyphase de la chaine du Karakoram (Baltoro, Nord Pakistan). Comptes Rendus de l'Académie des Sciences 303, 1611–1614.

Bertrand, J.M., Kienast, J.R., Pinardon, J.L., 1988. Structure and metamorphism of the Karakorum gneisses in the Braldu–Baltoro valley (north Pakistan). Geodinamica Acta 2, 135–150.

Bhalla, J.K., Bishui, P.K., Mathur, A.K., 1994. Geochronology and geochemistry of some granitoids of Kameng and Subansiri districts, Arunachal Pradesh. Indian Mineralogist 48, 61–76.

Boekhout, F., Roberts, N.M.W., Gerdes, A., Schaltegger, U., 2013. Continent formation in accretionary orogens: a Hf-isotope perspective on the Peruvian proto-Andes. Geological Society of London, Special Publication (389).

Bouilhol, P., Schaltegger, U., Chiaradia, M., Ovtcharova, M., Stracke, A., Burg, J.-P., Dawood, H., 2011. Timing of juvenile arc crust formation and evolution in the Sapat Complex (Kohistan–Pakistan). Chemical Geology 280, 243–256.

Bouilhol, P., Jagoutz, O., Hanchar, J.M., Dudas, F.O., 2013. Dating the India-Eurasia collision through arc magmatic records. Earth and Planetary Science Letters 366, 163–175.

Boutonnet, E., Leloup, P.H., Arnaud, N., Paquette, J.-L., Davis, W.J., Hattori, K., 2012. Synkinematic magmatism, heterogeneous deformation, and progressive strain localization in a strike-slip shear zone: the case of the right-lateral Karakorum fault. Tectonics 31, TC4012.

Buda, G., Dobosi, G., 2004. Lamprophyre-derived high-K mafic enc1aves in Variscan granitoids from the Mecsek Mts, (South Hungary). Neues Jahrbuch für Mineralogie-Abhandlungen. 180, 115–147.

Cecil, M.R., Gehrels, G., Patchett, J., Ducea, M., 2011. U–Pb–Hf characterization of the central Coast Mountains batholith: implications for petrogenesis and crustal architecture. Lithosphere 3, 247–260.

Chappell, B.W., Bryant, C.J., Wyborn, D., 2012. Peraluminous I-type granites. Lithos 153, 142–153.

Chemenda, A.I., Jean-Pierre Burg, J.P., Mattauer, M., 2000. Evolutionary model of the Himalaya–Tibet system: geopoem based on new modelling, geological and geophysical data. Earth and Planetary Science Letters 174, 397–409.
Chiu, H.Y., Chung, S.L., Wu, F.Y., Liu, D., Liang, Y.H., Lin, I.J., Iizuka, Y., Xie, L.W., Wang, Y., Chu, M.F., 2009. Zircon U–Pb and Hf isotopic constraints from eastern Trans-Himalayan batholiths on the precollisional magmatic and tectonic evolution in southern Tibet. Tectonophysics 477, 3–19.
Chu, M.F., Chung, S.L., Song, B., Liu, D., O'Reilly, S.Y., Pearson, N.J., Ji, J., Wen, D.J., 2006. Zircon U–Pb and Hf isotope constraints on the Mesozoic tectonics and crustal evolution of southern Tibet. Geology 34, 745–748.
Chung, S.-L., Chu, M.F., Zhang, Y., Xie, Y., Lo, C.-H., Lee, T.Y., Lan, C.Y., Li, X., Zhang, Q., Wang, Y., 2005. Tibetan tectonic evolution inferred from spatial and temporal variations in post-collisional magmatism. Earth Science Reviews 68, 173–196.
Clemens, J.D., Wall, V.J., 1981. Origin and crystallization of some peraluminous (S-type) granitic magmas. The Canadian Mineralogist 19, 111–131.
Clemens, J.D., Stevens, G., Farina, F., 2011. The enigmatic sources of I-type granites: the peritectic connexion. Lithos 126, 174–181.
Coward, M.P., Jan, M.Q., Rex, D.C., Tarney, J., Thirwal, F., Windley, B.F., 1982. Geotectonic framework of the Himalaya of N. Pakistan. Journal of the Geological Society of London 139, 299–308.
Coward, M.P., Windley, B.F., Broughton, I.W., Luff, M.G., Petterson, M.G., Pudsey, C.J., Rex, D.C., Khan, M.A., 1986. Collision tectonics in the NW Himalayas. In: Coward, M.P., Ries, A.C. (Eds.), Collision Tectonics. Geological Society of London Special Publications, 19, pp. 203–219.
Crawford, M.B., Windley, B.F., 1990. Leucogranites of the Himalaya/Karakoram, magmatic evolution within collisional belts and the study of collision-related Leucogranite petrogenesis. In: Le Fort, P., Pearce, J.A., Pecher, A. (Eds.), Collision Magmatism. Journal of Volcanology and Geothermal Research, 44, pp. 1–19.
Crawford, M.B., Searle, M.P., 1992. Field relationships and geochemistry of pre-collisional (India–Asia) granitoid magmatism in the central Karakoram. Tectonophysics 206, 171–192.
Debon, F., Zimmermann, J.L., Bertrand, J.M., 1986. The Baltoro Granite (Karakoram axial batholith, northern Pakistan) an Upper Miocene subalkaline intrusion. Comptes Rendus de l'Académie des Sciences 303, 463–466.
Debon, F., Le Fort, P., Dautel, D., Sonet, J., Zimmermann, J.L., 1987. Granites of western Karakoram and northern Kohistan (Pakistan): a composite Mid-Cretaceous to upper Cenozoic magmatism. Lithos 20, 19–40.
Debon, F., Khan, N.A., 1996. Alkaline orogenic plutonism in the Karakoram batholith: the Upper Cretaceous Koz Sar complex (Karamber valley, N. Pakistan). Geodinamica Acta 9, 145–160.
Deniel, C., Vidal, P.H., Fernandez, A., Le Fort, P., Peucat, J.J., 1987. Isotopic study of the Manaslu granite (Himalaya, Nepal): inferences on the age and source of Himalayan Leucogranites. Contributions to Mineralogy and Petrology 96, 78–92.
Ding, L., Kapp, P., Zhong, D.L., Deng, W.M., 2003. Cenozoic volcanism in Tibet: evidence for a transition from oceanic to continental subduction. Journal of Petrology 44, 1833–1865.
De Sigoyer, J., Chavagnac, V., Blichert-Toft, J., Villa, I.M., Luais, B., Guillot, S., Cosca, M., Mascle, G., 2000. Dating the Indian continental subduction and collisional thickening in the northwest Himalaya: multichronology of the Tso Morari eclogites. Geology 28, 487–490.
Dewey, J.F., Cande, S.C., Pitman III, W.C., 1989. Tectonic evolution of the India–Eurasia collision zone. Eclogae Geologicae Helvetiae 82, 717–734.
Ferrara, G., Lombardo, B., Tonarini, S., Turi, B., 1991. Sr, Nd and O isotopic characterisation of the Gomphu La and Gumburanjun leucogranites (High Himalaya). Schweizerische Mineralogische und Petrographische Mitteilungen 71, 35–51.
Flowerdew, M.J., Millar, I.L., Vaughan, A.P.M., Horstwood, M.S.A., Fanning, C.M., 2006. The source of granitic gneisses and migmatites in the Antarctic Peninsula: a combined U–Pb SHRIMP and laser ablation Hf isotope study of complex zircons. Contributions to Mineralogy and Petrology 151, 751–768.
France-Lanord, C., Le Fort, P., 1988. Crustal melting and granite genesis during the Himalayan collision orogenesis. Transactions of the Royal Society of Edinburgh: Earth Sciences 79, 183–195.
Fraser, J.E., Searle, M.P., Parrish, R.R., Noble, S.R., 2001. Chronology of deformation, metamorphism, and magmatism in the southern Karakoram Mountains. Geological Society of America Bulletin 113, 1443–1455.
Frost, B.R., Arculus, R.J., Barnes, C.G., Collins, W.J., Ellis, D.J., Frost, C.D., 2001. A geochemical classification of granitic rocks. Journal of Petrology 42, 2033–2048.
Gaetani, M., Garzanti, E., 1991. Multi rifting history of North Indian plate margin and NW Himalaya. Bulletin of the American Association of Petroleum Geologists 75, 1397–1414.
Gaetani, M., 1997. The Karakoram Block in Central Asia, from Ordovician to Cretaceous. Sedimentary Geology 109, 339–359.
Gagnevin, D., Daly, J.S., Horstwood, M.S.A., Whitehouse, M.J., 2011. In-situ zircon U–Pb, oxygen and hafnium isotopic evidence for magma mixing and mantle metasomatism in the Tuscan Magmatic Province, Italy. Earth and Planetary Science Letters 305, 45–56.
Gehrels, G.E., Valencia, V.A., Ruiz, J., 2008. Enhanced precision, accuracy, efficiency, and spatial resolution of U–Pb ages by laser ablation-multicollector-inductively coupled plasma-mass spectrometry. Geochemistry, Geophysics, Geosystems 9, Q03017.
Goodge, J.W., Vervoort, J.D., 2006. Origin of Mesoproterozoic A-type granites in Laurentia: Hf isotope evidence. Earth and Planetary Science Letters 243, 711–731.
Goswami, S., Bhowmik, S.K., Dasgupta, S., 2009. Petrology of a non-classical Barrovian inverted metamorphic sequence from the western Arunachal Himalaya, India. Journal of Asian Earth Sciences 36, 390–406.
Green, O.R., Searle, M.P., Corfield, R.I., Corfield, R.M., 2008. Cretaceous–Tertiary carbonate platform evolution and the age of the India–Asia collision along the Ladakh Himalaya (Northwest India). Journal of Geology 116, 331–353.
Griffin, W.L., Wang, X., Jackson, S.E., Pearson, S.E., O'Reilly, S.Y., Xu, X.S., Zhou, X.M., 2002. Zircon chemistry and magma genesis, SE China: in-situ analysis of Hf isotopes, Pingtan and Tonglu igneous complexes. Lithos 61, 237–269.
Guo, Z., Wilson, M., 2012. The Himalayan leucogranites: constraints on the nature of their crustal source region and geodynamic setting. Gondwana Research 22, 360–376.
Harris, N., Inger, S., 1992. Trace element modelling of pelite derived granites. Contributions to Mineralogy and Petrology 110, 45–56.
Harris, N., Inger, S., Massey, J., 1993. The role of fluids in the formation of high Himalayan leucogranites. In: Searle, M.P., Treloar, P.J. (Eds.), Himalayan Tectonics. Geological Society of London, Special Publication, 74, pp. 391–400 (London).
Harris, N., Ayres, M., Massey, J., 1995. The incongruent melting of Muscovite: implications for the geochemistry and extraction of granite magmas. Journal of Geophysical Research 100, 15777–15787.
Harrison, T.M., Grove, M., Lovera, O.M., Catlos, E.J., D'andrea, J., 1999. The origin of Himalayan anatexis and inverted metamorphism: models and constraints. Journal of Asian Earth Sciences 17, 755–772.
Hawkesworth, C., Kemp, T., 2006. Using hafnium and oxygen isotopes in zircons to unravel the record of crustal evolution. Chemical Geology 226, 144–162.
Heuberger, S., Schaltegger, U., Burg, J.-P., Villa, I.M., Frank, M., Dawood, H., Hussain, S., Zanchi, A., 2007. Age and isotopic constraints on magmatism along the Karakoram–Kohistan suture zone, NW Pakistan. Evidence for subduction and continued convergence after India–Asia collision. Swiss Journal of Geosciences 100, 85–107.
Horton, F., Leech, M.L., 2013. Age and origin of granites in the Karakoram shear zone and Greater Himalaya Sequence, NW India. Lithosphere 5, 300–320.
Inger, S., Harris, N., 1993. Geochemical constraints on leucogranite magmatism in the Langthan Valley, Nepal Himalaya. Journal of Petrology 34, 345–368.
Jan, M.Q., Howie, R.A., 1981. The mineralogy and geochemistry of the metamorphosed basic and ultrabasic rocks of the Jijal complex, Kohistan, NW Pakistan. Journal of Petrology 22, 85–126.
Kemp, A.I.S., Hawkesworth, C.J., 2003. Granitic perspectives on the generation and secular evolution of the continental crust. In: Holland, H.D., Turekian, K.K. (Eds.), Treatise on Geochemistry—The Crust. Elsevier, Oxford, pp. 349–410.
Kemp, A.I.S., Wormald, R.J., Whitehouse, M.J., Price, R.C., 2005. Hf isotopes in zircon reveal contrasting sources and crystallization histories for alkaline to peralkaline granites of Temora, southeastern Australia. Geology 33, 797–800.
Kemp, A.I.S., Hawkesworth, C.J., Paterson, B.A., Kinny, P.D., 2006. Episodic growth of the Gondwana supercontinent from hafnium and oxygen isotopes in zircon. Nature 439, 580–583.
Kemp, A.I.S., Hawkesworth, C.J., Foster, G.L., Paterson, B.A., Woodhead, J.D., Hergt, J.M., Gray, C.M., Whitehouse, M.J., 2007. Magmatic and crustal differentiation history of granitic rocks from Hf–O isotopes in zircon. Science 315, 980–983.
Kemp, A.I.S., Hawkesworth, C.J., Paterson, B.A., Foster, G.L., Kinny, P.D., Whitehouse, M.J., Maas, R., EIMF, 2008. Exploring the plutonicvolcanic link: a zircon U–Pb, Lu–Hf and O isotope study of paired volcanic and granitic units from Southeastern Australia. Special Issue Plutons and Batholiths, The Wallace Pitcher Memorial Volume. Transactions of the Royal Society of Edinburgh, Earth Science, 97, pp. 337–355.
Kemp, A.I.S., Foster, G.L., Scherstén, A., Whitehouse, M.J., Darling, J., Storey, C., 2009a. Concurrent Pb–Hf isotope analysis of zircon by laser ablation multi-collector ICP-MS, with implications for the crustal evolution of Greenland and the Himalayas. Chemical Geology 261, 244–260.
Kemp, A.I.S., Hawkesworth, C.J., Collins, W.J., Gray, C.M., Blevin, P.L., EIMF, 2009b. Isotopic evidence for rapid continental growth in an extensional accretionary orogen: the Tasmanides, eastern Australia. Earth and Planetary Science Letters 284, 455–466.
Kita, N.T., Ushikuzeho, T., Fu, B., Valley, J.W., 2009. High precision SIMS oxygen isotope analyses and the effect of sample topography. Chemical Geology 264, 43–57.
Le Breton, N., Thompson, A.B., 1988. Fluid-absent (dehydration) melting of biotite in metapelites in the early stages of crustal anatexis. Contributions to Mineralogy and Petrology 99, 226–237.
Leech, M.L., 2008. Does the Karakoram fault interrupt mid-crustal channel flow in the western Himalaya? Earth and Planetary Science Letters 276, 314–322.
Le Fort, P., Cuney, M., Deniel, C., Lanords, C.F., Sheppard, N.F., Upreti, B.N., Vidal, P., 1987a. Crustal generation of the Himalayan leucogranite. Tectonophysics 134, 39–57.
Le Fort, P., Michard, A., Sonet, J., Zimmermann, J.L., 1983. Petrography, geochemistry and geochronology of some samples from the Karakoram axial batholith (Northern Pakistan). In: Shams, F.A. (Ed.), Granites of the Himalaya, Karakoram and Hindu Kush. Lahore University, Pakistan, pp. 377–387.
Le Fort, P., Cuney, M., Deniel, C., Lanords, C.F., Sheppard, N.F., Upreti, B.N., Vidal, P., 1987b. Crustal generation of the Himalayan leucogranite. Tectonophysics 134, 39–57.
Leier, A.L., Kapp, P., Gehrels, G.E., DeCelles, P.G., 2007. Detrital zircon geochronology of Carboniferous–Cretaceous strata in the Lhasa terrane, southern Tibet. Basin Research 19, 361–378.
Leloup, P.H., Boutonnet, E., Davis, W.J., Hattori, K., 2011. Long-lasting intracontinental strike-slip faulting: new evidence from the Karakorum shear zone in the Himalayas. Terra Nova 23, 92–99.
Le Maitre, R.W., Bateman, E., Dudek, P., Keller, A., Lameyre, J., Le Bas, J., Sabine, M.J., Schmid, P.A., Sorensen, R., Streckeisen, H., Woolley, A.R., Zanettin, B., 1989. A Classification of Igneous Rocks and Glossary of Terms, Recommendations of the International Union of Geological Sciences, Subcommission on the Systematics of Igneous Rocks. Blackwell Scientific, Oxford.
Lemennicier, Y., Le Fort, P., Lombardo, B., Pêcher, A., Rolfo, F., 1996. Tectonometamorphic evolution of the central Karakorum (Baltistan — northern Pakistan). Tectonophysics 260, 119–143.
Liu, D., Zhao, Z., Zhu, D.C., Niu, Y., Harrison, T.M., 2014. Zircon xenocrysts in Tibetan ultrapotassic magmas: imaging the deep crust through time. Geology 42, 43–46.

Mahar, M.A., Mahéo, G., Goodell, P.C., Pavlis, T.L., 2014. Timing and origin of migmatitic gneisses in south Karakoram: insights from U–Pb, Hf and oxygen isotopic record of zircons (submitted for publication).
Mahéo, G., Guillot, S., Blichert-Toft, J., Rolland, Y., Pêcher, A., 2002. A slab breakoff model for the Neogene thermal evolution of South Karakoram and South Tibet. Earth and Planetary Science Letters 195, 45–58.
Mahéo, G., Pêcher, A., Guillot, S., Rolland, Y., Delacourt, C., 2004. Exhumation of Neogene gneiss domes between oblique crustal boundary in South Karakoram (NW Himalaya, Pakistan). In: Whitney, D.L., Teyssier, V., Siddoway, C.S. (Eds.), Gneiss Domes in Orogeny. Geological Society of America, Special Papers, 380, pp. 141–154.
Mahéo, G., Blichert-Toft, J., Pin, C., Guillot, S., Pêcher, A., 2009. Partial melting of mantle and crustal sources beneath South Karakoram, Pakistan: implications for the Miocene geodynamic evolution of the India–Asia convergence zone. Journal of Petrology 50, 427–449.
Maniar, P.D., Piccoli, P.M., 1989. Tectonic discrimination of granitoids. Geological Society of America Bulletin 101, 635–643.
Miles, A., Graham, C., Hawkesworth, C., Gillespie, M., Dhuime, B., Hinton, R., 2014. Using zircon isotope compositions to constrain crustal structure and pluton evolution: the Iapetus Suture Zone granites in northern Britain. Journal of Petrology 55, 181–207.
Miller, C., Schuster, R., Klötzli, U., Frank, W., Purtscheller, F., 1999. Post-collisional potassic and ultrapotassic magmatism in SW Tibet: geochemical and Sr–Nd–Pb–O isotopic constrains for mantle source characteristics and petrogenesis. Journal of Petrology 40, 1399–1424.
Parrish, R.R., Tirrul, R., 1989. U–Pb age of the Baltoro granite, northwest Himalaya, and implications for zircon inheritance and monazite U–Pb systematics. Geology 17, 1076–1079.
Patiño Douce, A.E., Harris, N., 1998. Experimental constraints on Himalayan anatexis. Journal of Petrology 39, 689–710.
Patriat, P., Achache, J., 1984. India–Eurasia collision and chronology as implications for crustal shortening and driving mechanisms of plates. Nature 311, 615–621.
Pêcher, A., Seeber, L., Guillot, S., Jouanne, F., Kausar, A., Latif, M., Majid, A., Mahéo, G., Mugnier, J.L., Rolland, Y., van der Beek, P., Van Melle, J., 2008. Stress field evolution in the northwest Himalayan syntaxis, northern Pakistan. Tectonics 27, TC6005.
Petford, N., Atherton, M., 1996. Na-rich partial melts from newly underplated basaltic crust: the Cordillera Blanca Batholith, Peru. Journal of Petrology 37, 1491–1521.
Petterson, M.G., Windley, B.F., 1992. The field relationships, geochemistry and petrogenesis of the Cretaceous basalt Jutal dyke suite, Kohistan, N. Pakistan. Journal of the Geological Society of London 149, 107–114.
Phillips, G., Landenberger, B., Belousova, E.A., 2011. Building the New England Batholith, eastern Australia-linking granite petrology with geodynamic setting using Hf isotopes in zircon. Lithos 122, 1–12.
Pognante, U., 1992. Migmatites and leucogranites of Tertiary age from the Higher Himalayan crystallines of Zanskar (NW India): a case of anatexis of Palaeozoic orthogneiss. Mineralogy and Petrology 46, 291–313.
Rapp, R.P., Watson, E.B., 1995. Dehydration melting of metabasalt at 8–32 kbar: implications for continental growth and crust–mantle recycling. Journal of Petrology 36, 891–931.
Ravikant, V., 2006. Utility of Rb–Sr geochronology in constraining Miocene and Cretaceous events in the eastern Karakoram, Ladakh, India. Journal of Asian Earth Sciences 27, 534–543.
Ravikant, V., Wu, F., Ji, W., 2009. Zircon U–Pb and Hf isotopic constraints on petrogenesis of the Cretaceous–Tertiary granites in eastern Karakoram and Ladakh, India. Lithos 110, 153–166.
Reichardt, H., Weinberg, R.F., Andersson, U.B., Fanning, C.M., 2010. Hybridization of granitic magmas in the source: the origin of the Karakoram Batholith, Ladakh, NW India. Lithos 116, 249–272.
Rex, A.J., Searle, M.P., Tirrul, R., Crawford, M.B., Prior, D.J., Rex, D.C., Barnicoat, A., Bertrand, J.-M., 1988. The geochemical and tectonic evolution of the central Karakoram, north Pakistan. Philosophical Transactions of the Royal Society of London, Series A 326, 229–255.
Richards, A., Argles, T., Harris, N., Parrish, R., Ahmad, T., Darbyshire, F., Draganits, E., 2005. Himalayan architecture constrained by isotopic tracers from clastic sediments. Earth and Planetary Science Letters 236, 773–796.
Rolland, Y., Pêcher, A., Picard, C., 2000. Middle Cretaceous back-arc formation and arc evolution along the Asian margin: the Shyok Suture Zone in northern Ladakh (NW Himalaya). Tectonophysics 325, 145–173.
Rolland, Y., Mahéo, G., Guillot, S., Pêcher, A., 2001. Tectono-metamorphic evolution of the Karakoram Metamorphic Complex (Dassu–Askole area, NE Pakistan): exhumation of mid-crustal HT–MP gneisses in a convergent context. Journal of Metamorphic Geology 19, 717–737.
Rolland, Y., Pêcher, A., Picard, C., Lapierre, H., Bosch, D., Keller, F., 2002. The Ladakh Arc of NW Himalaya — slab melting and melt–mantle interaction during fast northward drift of Indian Plate. Chemical Geology 182, 139–178.
Schaltegger, U., Zeilinger, G., Frank, M., Burg, J.P., 2002. Multiple mantle sources during island arc magmatism: U–Pb and Hf isotopic evidence from the Kohistan arc complex, Pakistan. Terra Nova 14, 461–468.
Schärer, U., Copeland, P., Harrison, T.M., Searle, M.P., 1990. Age, cooling history and origin of postcollisional leucogranites in the Karakoram batholith, a multisystem isotope study. Journal of Geology 98, 233–251.
Searle, M.P., Windley, B.F., Coward, M.P., Cooper, D.J.W., Rex, A.J., Rex, D.C., Tingdong, Li, Xuchang, Xiao, Jan, M.Q., Thakur, V.C., Kumar, S., 1987. The closing of Tethys and the tectonics of the Himalayas. Geological Society of America Bulletin 98, 678–701.
Searle, M.P., Rex, A.J., Tirrul, R., Rex, D.C., Barnicoat, A., Windley, B.F., 1989. Metamorphic, magmatic and tectonic evolution of the central Karakoram in the Biafo–Baltoro–Hushe regions of northern Pakistan. Geological Society of America, Special Paper 232, 47–74.
Searle, M.P., Crawford, M.B., Rex, A.J., 1992. Field relations, geochemistry, origin and emplacement of the Baltoro granite, Central Karakorum. Transactions of the Royal Society of Edinburgh: Earth Sciences 83, 519–538.
Searle, M.P., Parrish, R.R., Hodges, K.V., Hurford, A., Ayres, M.W., Whitehouse, M.J., 1997. Shisha Pangma leucogranite, South Tibetan Himalaya: field relations, geochemistry, age, origin and emplacement. Journal of Geology 105, 295–317.
Searle, M.P., Weinberg, R.F., Dunlap, W.J., 1998. Transpressional tectonics along the Karakoram fault zone, northern Ladakh: constraints on Tibetan extrusion. In: Holdsworth, R.E., Strachan, R.A., Dewey, J.F. (Eds.), Continental Transpressional and Transtensional Tectonics. Geological Society of London Special Publication, 135, pp. 307–326.
Searle, M.P., Waters, D.J., Dransfield, M.W., Stephenson, B.J., Walker, C.B., Walker, J.D., Rex, D.C., 1999. Thermal and mechanical models for the structural and metamorphic evolution of the Zanskar High Himalaya. In: Mac Niocaill, C., Ryan, P.D. (Eds.), Continental Tectonics. Geological Society of London Special Publication, 164, pp. 139–156.
Searle, M.P., Phillips, R.J., 2007. Relationships between right-lateral shear along the Karakoram Fault and metamorphism, magmatism, exhumation and uplift: evidence from the K2–Gasherbrum–Pangong Ranges, north Pakistan and Ladakh. Journal of the Geological Society, London 164, 439–450.
Searle, M.P., Parrish, R.R., Thow, A.V., Noble, S., Phillips, R.J., Waters, D.J., 2010. Anatomy, age and evolution of a collisional mountain belt: the Baltoro granite batholith and Ka rakoram Metamorphic Complex, Pakistani Karakoram. Journal of the Geological Society 167, 183–202.
Sen, C., Dunn, T., 1994. Dehydration melting of a basaltic composition amphibolite at 1.5 and 2.0 GPa: implications for the origin of adakites. Contributions to Mineralogy and Petrology 117, 394–409.
Shaw, S.E., Flood, R.H., 2009. Zircon Hf isotopic evidence for mixing of crustal and silicic mantle-derived magmas in a zoned granite pluton, eastern Australia. Journal of Petrology 50, 147–168.
Singh, R.K.B., 2013. Origin and emplacement of the Higher Himalayan leucogranite in the eastern Himalaya: constraints from geochemistry and mineral chemistry. Journal of the Geological Society of India 81, 791–803.
Srimal, N., Basu, A.R., Kyser, T.K., 1987. Tectonic inferences from oxygen isotopes in volcano-plutonic complexes of the India–Asia collision zone, NW India. Tectonics 6, 261–273.
Stuckless, J.S., 1989. Petrogenesis of two contrasting late Archean granitoids, Wind River Range, Wyoming. USGS Professional paper, 1491, pp. 1–38.
Thompson, A.B., 1982. Dehydration melting of pelitic rocks and the generation of H_2O undersaturated granitic liquids. American Journal of Science 282, 1567–1595.
Thompson, A.B., Connolly, J.A.D., 1995. Melting of the continental crust; some thermal and petrological constraints on anatexis in continental collision zones and other tectonic settings. Journal of Geophysical Research 100, 15565–15579.
Todd, V.R., Shaw, S.E., 1985. S-type granitoids and an I–S line in the Penisular Ranges Batholith, Southern California. Geology 13, 231–233.
Treloar, P.J., Rex, D.C., Guise, P.G., Coward, M.P., Searle, M.P., Windley, B.F., Petterson, M.G., Jan, M.Q., Luff, I.W., 1989. K–Ar and Ar–Ar geochronology of the Himalayan collision in NW Pakistan: constraints on the timing of suturing, deformation, metamorphism and uplift. Tectonics 8, 881–909.
Turner, S., Arnaud, N., Liu, J., Rogers, N., Hawkesworth, C.N., Harris, S.K., Van Calsteren, P., Deng, W., 1996. Post-collision, shoshonitic volcanism on theTibetan Plateau: implications for convective thinning of the lithosphere and source of ocean island basalt. Journal of Petrology 37, 45–71.
Valley, J.W., 2003. Oxygen isotopes in zircon. In: Hanchar, J.M., Hoskin, P.W.O. (Eds.), Zircon. Reviews in Mineralogy and Geochemistry, 53, pp. 343–386.
Valley, J.W., Lackey, J.S., Cavosie, A.J., Clechenko, C.C., Spicuzza, M.J., Basei, M.A.S., Bindeman, I.N., Ferreira, V.P., Sial, A.N., King, E.M., Peck, W.H., Sinha, A.K., Wei, C.S., 2005. 4.4 billion years of crustal maturation: oxygen isotope ratios of magmatic zircon. Contributions to Mineralogy and Petrology 150, 561–580.
Valley, J.W., Kita, N.T., 2009. In situ oxygen isotope geochemistry by ion microprobe. In: Fayek, M. (Ed.), MAC Short Course. Secondary Ion Mass Spectrometry in the Earth Sciences, 41. Mineralogical Association of Canada, pp. 19–63.
Van de Zedde, D.M.A., Wortel, M.J.R., 2001. Shallow slab detachment as a transient source of heat at midlithospheric depths. Tectonics 20, 868–882.
Vielzeuf, D., Schmidt, M.W., 2001. Melting relations in hydrous systems revisited: application to metapelites, metagreywackes and metabasalts. Contributions to Mineralogy and Petrology 141, 251–267.
Visona, D., Lombardo, B., 2002. Two-mica and tourmaline leucogranites from the Everest–Makalu region (Nepal–Tibet): Himalayan leucogranite genesis by isobaric heating? Lithos 62, 125–150.
Weinberg, R.F., Dunlap, W., Whitehouse, M., 2000. New field, structural and geochronological data from the Shyok and Nubra valleys, northern Ladakh: linking Kohistan to Tibet. In: Khan, M.A., Treloar, P.J., Searle, M.P., Jan, M.Q. (Eds.), Tectonics of the Nanga Parbat Syntaxis and the Western Himalaya. Geological Society London Special Publications, 170, pp. 253–275.
Weinberg, R.F., Mark, G., Reichardt, H., 2009. Magma ponding in the Karakoram shear zone, Ladakh, NW India. Geological Society of America Bulletin 121, 278–285.
Williams, H.M., Turner, S.P., Pearce, J.A., Kelley, S.P., Harris, N.B.W., 2004. Nature of the source regions for post-collisional, potassic magmatism in southern and northern Tibet from geochemical variations and inverse trace element modelling. Journal of Petrology 45, 555–607.
Wu, F., Clift, P.D., Yang, J., 2007. Zircon Hf isotopic constraints on the sources of the Indus Molasse, Ladakh Himalaya, India. Tectonics 26, TC2014.

Zeh, A., Gerdes, A., Klemd, R., Barton Jr., J.M., 2007. Archaean to Proterozoic crustal evolution in the Central Zone of the Limpopo Belt (South Africa/Botswana): constraints from combined U–Pb and Lu–Hf isotope analyses of zircon. Journal of Petrology 48, 1605–1639.

Zhang, H.F., Xu, W.C., Guo, K.Q., Cai, H.M., Yuan, H.L., 2007. Zircon U–Pb and Hf isotopic composition of deformed granite in the southern margin of the Gangdese belt, Tibet: evidence for early Jurassic subduction of Neo-Tethyan oceanic slab (in Chinese with English abstract) Acta Petrologica Sinica 23, 1347–1353.

Zhu, B., Kidd, W.S.F., Rowley, D.B., Currie, B.S., Shafique, N., 2005. Age of initiation of the India–Asia collision in the east central Himalaya. Journal of Geology 113, 265–285.